Title
THEORY OP THE rf MANIFOLD AND MEASUREMENTS ON A MODEL MANIFOLD SYSTEM

Author
Voelker, Ferdinand.

Publication Date
1967-04-01

UCRL-17508

ey. 2

University of California

Ernest O. Lawrence Radiation Laboratory

THEORY OF THE rf MANIFOLD AND MEASUREMENTS ON A MODEL MANIFOLD SYSTEM

Ferdinand Voelker

April 1967

DISCLAIMER

UCRL-17508
UC-28
Particle Accel. and
High Volt. Mach.
TID-4500 (50th Ed.)

UNIVERSITY OF CALIFORNIA

Lawrence Radiation Laboratory
Berkeley, California

AEC Contract No. W-7405-eng-48

THEORY OF THE rf MANIFOLD AND MEASUREMENTS ON A MODEL MANIFOLD SYSTEM

Ferdinand Voelker

April 1967

Printed in the United States of America
Available from
Clearinghouse for Federal Scientific and Technical Information
National Bureau of Standards, U.S. Department of Commerce
Springfield, Virginia 22151
Price: Printed Copy $3.00; Microfiche $0.65

THEORY OF THE rf MANIFOLD AND MEASUREMENTS ON A MODEL MANIFOLD SYSTEM

Ferdinand Voelker

Lawrence Radiation Laboratory
University of California
Berkeley, California

April 1967

ABSTRACT

We are proposing a system to distribute rf energy to a linear accelerator from an adjacent manifold. This system is described and a simple theory is developed to show that the voltage will be "locked" in the various load cavities. A method is developed to predict the frequency of adjacent modes. Various predicted values are compared with experimental results from a model rf manifold.

I. INTRODUCTION

The source of radio-frequency power is one of the major parts of a linear accelerator, and it is desirable to have an rf system that is reliable and flexible without being unduly expensive. A 200 MeV proton linac, under consideration as part of the injection system for a 200 GeV synchrotron, will consist of a number of rf cavities. We have devised a system, an rf manifold, that pools all the rf amplifiers to supply all the cavities as a common load. The system uses a particular distribution network that holds the fields in the rf cavities to close tolerances while the beam-loading changes. It makes rf energy available along the linac, much as a water or vacuum manifold provides water or vacuum along its length. This is in contrast to a system in which each linac cavity is powered from a separate amplifier, each of which must have a separate fast voltage regulator and phase servo to synchronize the amplitudes and phases of the cavity fields.

A significant advantage of a manifold is the increase in reliability that it makes possible. For a 200 MHz linac, the unit of rf power will be a 5-MW amplifier. Four to eight amplifiers will be needed, depending on the beam loading. It is relatively inexpensive to include one or two more amplifiers at the manifold as on-line spares. Then it would require only a suitable disconnect switch in the coupling line to remove a faulty tube. This could be done very rapidly with almost negligible down time, and without affecting the rest of the system. If the on-line spares are delivering their share of power, all the amplifiers normally operate at 75% of rated power, and this also substantially increases reliability. There is additional inherent reliability because the locking of amplitude and phase throughout the system is achieved by a passive network that is as stable as the mechanical dimensions, thus eliminating the complexity of a fast voltage regulator and phase servo for each cavity.

There is also much inherent flexibility in a manifold system. Power can be removed or added along the length without affecting the operation. There is a definite advantage in making the cavities short, because then the nearest modes in the cavities are separated farther in frequency, which relieves the mechanical tolerances in the cavities. Since the cavities do not have to be tailored to the amplifier tube size, one amplifier can power several rf cavities. We are planning cavities approximately 7.5 m long. Without beam, the power dissipated in the cavities varies from 0.4 MW at the input

end to 1.4 MW at the output end. Conventional Alvarez linac cavities operate at the cutoff frequency. On this cutoff mode, the amplitude and phase of the rf fields vary with the distance from the rf feed point, and the amount of variation depends on the beam current.[1,2] The 7.5-meter cavities proposed are short enough that, with a single feed point in the center, the fields will stay within tolerance over the length of the cavities for beam currents of the order of 100 mA. If it is desired to use longer cavities, the field variation along the length of the cavities can be held within acceptable limits either by using several feed points connected to different points in the manifold or by using one of the recently developed cavity structures that effectively operates in the center of a passband.[3-5]

During the initial operation of a linac cavity it is desirable to have a large amount of excess rf power available to break through multipactoring. A manifold system allows several amplifiers to be connected to a single cavity to provide as much excess power as necessary. In our linac we are planning to use 5 MW amplifiers and 1 MW cavity loads; thus only one amplifier is needed when the system is first being debugged. One cavity at a time can be coupled to the manifold and processed until it holds voltage. As more rf power becomes necessary to operate the first few sections of linac, more amplifiers can be added, until eventually the whole linac is in service. Then as beam loading is increased, additional amplifiers can be connected to the manifold.

There is a potential disadvantage to a manifold system for some applications. Since all load points are electrically locked in amplitude, any change in individual cavity voltage with respect to the system has to be made mechanically by rotating a loop in the cavity. Similarly, since cavity fields are locked with respect to phase, coarse changes in phase between individual cavities and the beam must be made mechanically by moving the cavity along its length, so that the beam enters the tank at a different electrical phase. Fine phase adjustments can be made by changing the voltage level in the cavity. This precludes fast changes in one part of the system with respect to the rest of the system. It does not present any difficulty, however, in the linac we are planning.

Obviously some kind of transmission line (or waveguide) is necessary to carry rf power, and we next describe the constraints that make it behave like a manifold. The length of the manifold must be an integral number of

half wavelengths at the operating frequency. The manifold can be either linear or in the form of a ring, as is used on the DESY synchrotron.[6] Connection to the manifold must be made only at certain points that we call mesh points. Mesh points are defined as the positions along the manifold where the voltage maxima would occur if the unloaded manifold were excited at the operating frequency. At 200 MHz these occur every half-wave length or every 75 cm along a coaxial line; loads and amplifiers are connected to the nearest convenient mesh point. We show in Section II that if the loads are at the mesh points, the voltages are locked in phase and in amplitude at the operating frequency.

There are some other constraints on connection of loads and amplifiers to the system. Both cavity loads and amplifiers are resonant circuits which of necessity are somewhat distant from the manifold. The loads and amplifiers must be connected to the manifold through coupling transmission lines which are electrically multiples of $\lambda/2$ in length. This means that the detuned-short position of each coupling line must lie at the junction of the coupling line and the manifold. The detuned-short position is the point on the coupling line where one gets the tightest coupling to the cavity, and is discussed in more detail in Section III. We shall also show in Section III that there is voltage lock between the manifold and the cavity fields.

The manifold system works only at the one frequency for which it is designed, and must be driven from a crystal-controlled oscillator. Suitable mechanical tuners are used to servo the individual cavity resonances to this frequency. Since the beam is not in phase with the fields in the cavities, appreciable reactive energy must be supplied by the manifold and ultimately by the amplifiers. If two cavities are detuned in opposite directions from each other, each will supply reactive energy to the other through the manifold, and only the difference has to be supplied by the amplifier. If the prebuncher also is fed from the manifold, then the phase of the fundamental component of beam will be locked with respect to the phase of the cavity fields, and it does not matter that the phase of the system changes with respect to the amplifier drive. The change of the system phase with respect to the amplifier drive voltage causes the amplifiers to supply automatically whatever reactive energy is necessary to keep the system in resonance at the cost of additional anode dissipation in the amplifier tubes. There are two alternatives to designing additional peak anode dissipation into the system. One is to tune

the system so that the amplifiers supply minimum reactive energy and maximum resistive energy during the time that the beam is on, and to let the system be detuned when the beam is off and the demand for resistive energy is reduced. Another alternative is to servo the reference phase during the pulse, which would require one fast-phase servo. These are alternatives of efficiency versus complexity, and the choice may be determined by the amount of beam loading.

The beam will extract stored energy from the cavity, which will act as a filter to smooth out the demand for new energy from the manifold. The rate at which energy is needed at the cavities is small compared with the rate at which it can be propagated from the nearest amplifier, but there will be transient voltages caused by shock excitation of the adjacent modes of the system; this subject is dealt with in Section V. Since the extra energy being extracted by the beam causes the system voltage to decrease, it must be compensated for by a voltage regulator that controls the power output of the amplifiers. A particular mesh point can be chosen as a reference, and the system can be regulated by controlling the voltage at this mesh point.

The basic theory of the rf manifold is explained in the first four parts of this paper. Sections II and III deal with amplitude and phase lock along the manifold, and between the manifold and the cavity fields, respectively. Section IV deals with adjacent modes in the operating passband, and Section V describes briefly the relationship between these modes and some of the transient phenomena. At Lawrence Radiation Laboratory we have set up a one-tenth length rf manifold system feeding six cavity loads to check our theory on a working model. Section VI is a description of the model manifold and the operating procedure. Section VII deals with a comparison between the theory and measurements that have been made on the model manifold.

II. AMPLITUDE AND PHASE LOCK ON THE MANIFOLD

Let us treat the manifold as a series of transmission-line sections loaded at each end. We shall consider the properties of one section; we can then analyze the manifold section by section. First we find equations in terms of an arbitrary load admittance, and then substitute an expression to represent the cavity load. To simplify the algebra, the load is divided with the same loading on both sides of the section, as shown in Fig. 1. The two adjacent load points are $m+1$ and m. Writing a transmission matrix[7] for each element in the section and multiplying these together gives a product matrix, which relates voltage and current at each load point:

$$\begin{bmatrix} V_{m+1} \\ I_{m+1} \end{bmatrix} = \begin{bmatrix} 1 & 0 \\ \frac{Y_L}{2} & 1 \end{bmatrix} \begin{bmatrix} \cosh\gamma\ell & \frac{1}{Y_0}\sinh\gamma\ell \\ Y_0 \sinh\gamma\ell & \cosh\gamma\ell \end{bmatrix} \begin{bmatrix} 1 & 0 \\ \frac{Y_L}{2} & 1 \end{bmatrix} \begin{bmatrix} V_m \\ I_m \end{bmatrix}$$

or

$$\begin{bmatrix} V_{m+1} \\ I_{m+1} \end{bmatrix} = \begin{bmatrix} \cosh\gamma\ell + \frac{Y_L}{2Y_0}\sinh\gamma\ell & \frac{1}{Y_0}\sinh\gamma\ell \\ Y_L\cosh\gamma\ell + \left(Y_0 + \frac{Y_L^2}{4Y_0}\right)\sinh\gamma\ell & \cosh\gamma\ell + \frac{Y_L}{2Y_0}\sinh\gamma\ell \end{bmatrix} \begin{bmatrix} V_m \\ I_m \end{bmatrix}. \tag{1}$$

The line parameters are Y_0 and $\gamma \equiv \alpha + j\beta$. The length of line between load points is ℓ and the load admittance is Y_L. These do not have to be the same for each section, but we will leave off identifying subscripts to simplify the notation. Let us assume the losses are low, so that $\alpha\ell << 1$. The matrix equation can be rewritten to give

$$V_{m+1} = \left(\cosh\gamma\ell + \frac{Y_L}{2Y_0}\sinh\gamma\ell\right) V_m + \left(\frac{1}{Y_0}\sinh\gamma\ell\right) I_m, \tag{2}$$

$$I_{m+1} = \left[Y_L\cosh\gamma\ell + \left(Y_0 + \frac{Y_L^2}{4Y_0}\right)\sinh\gamma\ell\right] V_m + \left(\cosh\gamma\ell + \frac{Y_L}{2Y_0}\sinh\gamma\ell\right) I_m. \tag{3}$$

Since the nominal distance between load points is $n\lambda/2$, the electrical length is $\beta\ell = n\pi + \delta_0 n\pi$, where δ_0 is a small quantity representing errors in length for a given section, and may be different for each section. Then to

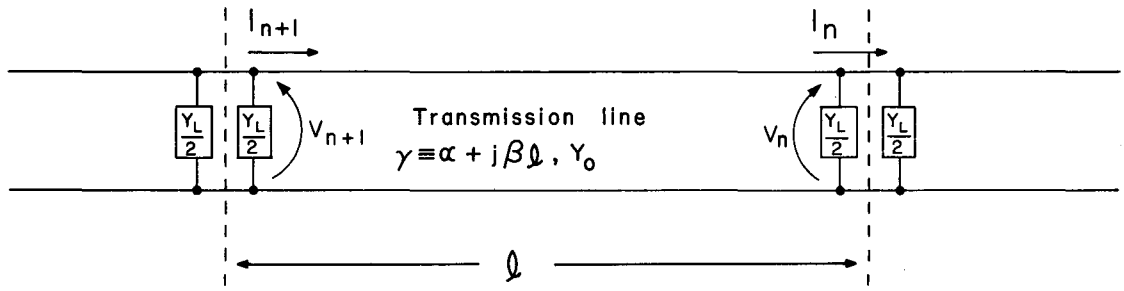

Fig. 1. One section of manifold system.

first order in δ_0,

$$\cosh\gamma\ell \approx (1 + j\,\alpha\ell\,\delta_0 n\pi)\cos n\pi ,$$

$$\sinh\gamma\ell \approx (\alpha\ell + j\,\delta_0 n\pi)\cos n\pi .$$

The factor $\cos n\pi$ is either +1 or -1 depending on whether the section is an even or odd number of $\lambda/2$ in length. We shall show in Section III that the cavity load can be represented by the functional form

$$Y_L = G(1 + j\,2\delta_L Q) ,$$

where G is the real part of the shunt admittance, ω_0 is the resonant frequency of the load, and $2\delta_L \approx 1 - \omega_0^2/\omega^2$. Substituting Y_L and the above approximation into Eqs. (2) and (3), we find

$$V_{m+1} \approx \cos n\pi \left[\left\{ 1 + \alpha\ell \frac{G}{Y_0} - \delta_0 n\pi \frac{G\delta_L Q}{Y_0} + j\left(\alpha\ell \frac{G\delta_L Q}{Y_0} + \delta_0 n\pi \frac{G}{2Y_0} \right) \right\} V_m + \left\{ \alpha\ell + j\,\delta_0 n\pi \right\} \frac{I_m}{Y_0} \right] , \tag{4}$$

$$I_{m+1} \approx \cos n\pi \left[\left\{ G + \alpha\ell \left[Y_0 + \frac{G^2}{4Y_0} \left(1 - 4\delta_L^2 Q^2 \right) \right] - \delta_0 n\pi \frac{G\delta_L Q}{Y_0} \right\} V_m + \left\{ 1 + \alpha\ell \frac{G}{2Y_0} - \delta_0 n\pi \frac{G\delta_L Q}{Y_0} + j\left[\alpha\ell \frac{G\delta_L Q}{Y_0} + \delta_0 n\pi \frac{G}{2Y_0} \right] \right\} I_m . \tag{5}$$

Let us rearrange Eq. (4):

$$\frac{V_{m+1}}{V_m} = 1 + \left[\frac{\alpha\ell}{Y_0} \left(\frac{G}{2} + \frac{I_m}{V_m} \right) - \delta_0 n\pi \frac{G}{Y_0} \delta_L Q \right] + j\left[\frac{\alpha\ell}{Y_0} G\delta_L Q + \delta_0 \frac{n\pi}{Y_0} \left(\frac{G}{2} + \frac{I_m}{V_m} \right) \right] . \tag{6}$$

Both α and δ_0 are small near the operating frequency, and terms that are the product of these factors have been neglected. The $\cos n\pi$ factor can be cancelled by the orientation of the coupling loop in the cavity. Equation (6)

is of particular interest because it shows the variation in voltage from one load point to the next. Since the perturbing terms are quite small, the real terms are the deviation in amplitude and the imaginary terms are the deviation in phase.

The $\alpha\ell$ or loss terms cause deviation in both amplitude and phase. In general, α can be made smaller by increasing the cross section of the manifold, but in a 200 MHz coaxial line, we must restrict the diameter to 22 in. to prevent propagation of the next higher transmission-line mode. Since the cavities are about 7.5 meters long, $\alpha\ell \approx 10^{-4}$ per section.

Similarly the δ_0 terms cause deviation in both phase and amplitude. The quantity δ_0 is a measure of the error in electrical length in the manifold, which is due to an error either in frequency or in dimensions. Normally the operating frequency will be adjusted to make the average δ_0 equal to zero. Then any nonzero δ_0 terms are due to manufacturing or to temperature differences along the manifold. The manifold will be made of accurately machined sections, and if the manufacturing tolerances on the lengths can be held to less than 0.006 in. then $\delta_0 \leq 10^{-4}$. The manifold must have its temperature controlled to within several degrees C to keep δ_0 within tolerance.

Let us consider the other parameters in Eq. (6). We are planning a mesh-point voltage of 30 kV on a 30-ohm coaxial line. With a 1-MW load, $G = 2P/V^2 = 1/450$ mho. The current flowing at a mesh point is proportional to power flow. It is not necessarily in phase with the voltage at the mesh point, and will depend on the distribution of amplifiers and loads. However, the power in the manifold should not exceed 15 MW in our linac, so $|I_n|$ will be less than 500 A. The system will have a slow mechanical servo at each cavity to keep δ_L near zero when the beam is on. When the beam is off, $\delta_L Q$ will not exceed $\frac{1}{2}$. With $\ell \approx 7.5$ m, n = 10, and Eq. (6) becomes

$$\frac{V_{m+1}}{V_m} \approx 1 + 30\left[10^{-4}\left(\frac{1}{450}+\frac{1}{60}\right) + 10^{-4}\times 10\pi\times\frac{1}{900}\right] + j\,30\left[10^{-4}\times\frac{1}{900} + 10^{-4}\left(\frac{1}{450}+\frac{1}{60}\right)\right]$$

$$= 1 + 1.62\times 10^{-4} + j\,0.6\times 10^{-4}\,.$$

This corresponds to a change in amplitude of about 1 part in 6 000 and a change in phase per section of 0.0035 deg.

Voltage and current can be evaluated on a complete manifold system by starting at one end and calculating section by section. It is not necessary to carry along the perturbations in current for this calculation, since there is nothing analogous to voltage lock in the current equations, and Eq. (5) reduces to

$$I_{m+1} \approx \cos n\pi \left[G(1 + j\, 2\delta_L Q)\, V_m + I_m \right]. \qquad (7)$$

Each section that is evaluated can have a different length or load admittance, and in fact, some sections will have amplifiers instead of loads. Amplifiers are handled as loads with a negative value of G and a low value of Q corresponding to the amplifier resonator. The calculation becomes rather tedious if there are any detuned elements in the system, because at an arbitrary frequency, the boundary conditions are not necessarily satisfied at the end of the last section. One must keep repeating the calculation until a frequency is found that satisfies the boundary conditions. The only practical way to carry out a complete calculation of a complicated system is with a computer, and we have developed a program that enables us to calculate first the frequency that makes a given system resonant, and then to calculate voltage, power, standing-wave ratio, etc. at this frequency. With the computer we can use the trigonometric and hyperbolic functions instead of the first terms in the power-series expansion used to get the above equations, and some of the restrictions (such as $\delta_0 << 1$) do not apply to the computer solutions. This freedom makes the computer useful to search for other resonances in the operating passband. The computer program allows a different resonant frequency, power loss, and Q for each load, and it also allows different values of beam loading, and an arbitrary distribution of power from the amplifiers.

III. THE CAVITY LOAD AND COUPLING LINE

Next we want to show that there can be voltage lock between the manifold and the cavity if the proper constraints are made. If the linac sections are long Alvarez cavities with many resonances, the separation between resonances near the operating frequency is inversely proportional to the square of the length of the cavities. In Section IV we show that the operating mode in a manifold system is in the center of a narrow passband. It is desirable to make the cavities short enough so that the next cavity mode is

outside the operating passband. This requirement is easy to satisfy because rf power can be delivered in varying amounts along the manifold without affecting the operation; thus there is considerable flexibility in choosing the length of any linac cavity. We assume that the cavity acts like a single resonant circuit in the operating passband of the manifold. An equivalent circuit[8] of the manifold is shown in Fig. 2, where R, L, and C are parameters defining the linac cavity, and L_1 and M are parameters defining the loop. The cavity is connected to the manifold through a length ℓ_1 of coupling line with parameters Z_{01} and $\gamma_1 \equiv \alpha_1 + j\beta_1$. In this equivalent circuit V_c is the analog of the end-to-end voltage in the cavity. The beam is a repetitive current pulse that is shorter than one cycle of the rf drive frequency. Its Fourier component at the drive frequency is called I_b. The higher-frequency components will be swamped out in the large displacement current, and their main effect will be to distort the wave shape of the cavity fields slightly, unless they happen to coincide with a higher-order resonance of the cavity.

We want to make the voltage ratio between the cavity and the manifold independent of I_b and of the tuning of the cavity. If we take the product of the transmission matrices for the elements in Fig. 2, we get:

$$\begin{bmatrix} V_m \\ I_m \end{bmatrix} = \begin{bmatrix} \cosh\gamma_1\ell_1 & Z_{01}\sinh\gamma_1\ell_1 \\ \frac{1}{Z_{01}}\sinh\gamma_1\ell_1 & \cosh\gamma_1\ell_1 \end{bmatrix} \begin{bmatrix} 1 & SL_1 \\ 0 & 1 \end{bmatrix} \begin{bmatrix} 0 & -SM \\ \frac{1}{SM} & 0 \end{bmatrix} \begin{bmatrix} 1 & R+SL \\ 0 & 1 \end{bmatrix} \begin{bmatrix} 1 & 0 \\ SC & 1 \end{bmatrix} \begin{bmatrix} V_C \\ I_b \end{bmatrix} \tag{8}$$

or

$$\begin{bmatrix} V_m \\ I_m \end{bmatrix} = \begin{bmatrix} A & C \\ B & D \end{bmatrix} \begin{bmatrix} V_C \\ I_b \end{bmatrix} ,$$

where

$$A = -S^2MC\cosh\gamma_1\ell_1 + \frac{C}{M}\left(R+SL+\frac{1}{SC}\right)(SL_1\cosh\gamma_1\ell_1 + Z_{01}\sinh\gamma_1\ell_1) ,$$

$$B = -\frac{S^2MC}{Z_{01}}\sinh\gamma_1\ell_1 + \frac{C}{M}\left(R+SL+\frac{1}{SC}\right)\left(\frac{SL_1}{Z_{01}}\sinh\gamma_1\ell_1 + \cosh\gamma_1\ell_1\right) ,$$

$$C = -SM\cosh\gamma_1\ell_1 + \frac{R+SL}{SM}(SL_1\cosh\gamma_1\ell_1 + Z_{01}\sinh\gamma_1\ell_1) ,$$

$$D = -\frac{SM}{Z_{01}}\sinh\gamma_1\ell_1 + \frac{R+SL}{SM}\left(\frac{SL_1}{Z_{01}}\sinh\gamma_1\ell_1 + \cosh\gamma_1\ell_1\right) .$$

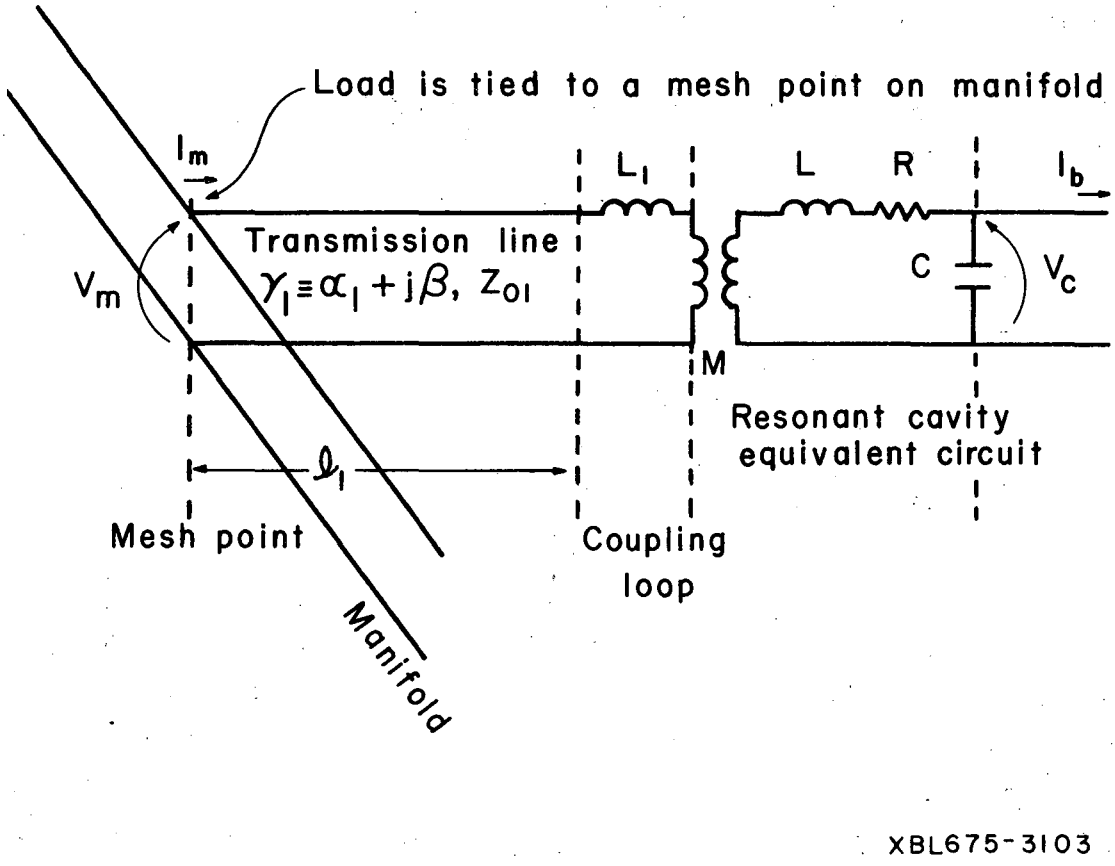

Fig. 2. Equivalent circuit of cavity and coupling system.

For the steady-state case $s = j\omega$. If the losses are low, $\alpha_1 \ell_1 << 1$, where $\gamma_1 \ell_1 \equiv \alpha_1 \ell_1 + j\beta_1 \ell_1$ in the coupling line. Then

$$\cosh \gamma_1 \ell_1 \approx \cos \beta_1 \ell_1 + j\, \alpha_1 \ell_1 \cdot \sin \beta_1 \ell_1 ,$$

$$\sinh \gamma_1 \ell_1 \approx \alpha_1 \ell_1 \cdot \cos \beta_1 \ell_1 + j \sin \beta_1 \ell_1 .$$

In Equation (8) the expression

$$sL_1 \cosh \gamma_1 \ell_1 + Z_{01} \sinh \gamma_1 \ell_1$$

becomes

$$\alpha_1 \ell_1 (Z_{01} \cos \beta_1 \ell_1 - \omega L_1 \sin \beta_1 \ell_1)$$
$$+ j (\omega L_1 \cos \beta_1 \ell_1 + Z_{01} \sin \beta_1 \ell_1) .$$

We choose the length of the coupling line ℓ_1 so that the imaginary part of this expression is zero. This is the same as saying that the detuned-short position on the coupling line falls at the junction of the manifold and the line. We shall see that this constraint causes voltage lock. We divide by $\cos \beta_1 \ell_1$, and define the parameter ξ, which measures how closely we have approached the ideal detuned-short restriction,

$$\xi \equiv \omega L_1 + Z_{01} \tan \beta_1 \ell_1 \to 0 . \tag{9}$$

Substitution of these expressions into Eq. (8) gives

$$\frac{V_m}{V_C} = \omega^2 MC \cos \beta_1 \ell_1 \left\{ (1 + j\, \alpha \ell_1 \tan \beta_1 \ell_1) \left(1 + \frac{I_b}{j\omega C V_c} \right) \right.$$
$$\left. + \left[\alpha_1 \ell_1 Z_{01} \frac{1}{\cos^2 \beta_1 \ell_1} + j\xi \right] \left[\frac{R + j\left(\omega L - \frac{1}{\omega C}\right)}{\omega^2 M^2} + \frac{I_b}{j\omega C V_c} \cdot \frac{R + j\omega L}{\omega^2 M^2} \right] \right\}, \tag{10}$$

$$\frac{I_m}{V_C} = \omega^2 MC \cos \beta_1 \ell_1 \left\{ \left(\alpha_1 \ell_1 + j \frac{\tan \beta_1 \ell_1}{Z_{01}} \right) \left(1 + \frac{I_b}{j\omega C V_c} \right) \right.$$
$$\left. + \left[Z_{01} \frac{1}{\cos^2 \beta_1 \ell_1} + j\, \alpha_1 \ell_1 \xi \right] \left[\frac{R + j\left(\omega L - \frac{1}{\omega C}\right)}{\omega^2 M^2} + \frac{I_b}{j\omega C V_c} \cdot \frac{R + j\omega L}{\omega^2 M^2} \right] \right\} \tag{11}$$

In these equations $\omega^2 MC \cos \beta_1 \ell_1$ is the voltage ratio between the manifold and the cavity. The expression $\left[R+j(\omega L- \frac{1}{\omega C})\right]/\omega^2 M^2$ is the admittance of the cavity transformed by the coupling loop. The factors $\alpha_1 \ell_1$ and ξ are small numbers that account for the loss and the misadjustment in length of the coupling line. Now $j\omega CV_c$ is the displacement current across the cavity gap, and it is of the order of Q times I_b. With $Q > 40\,000$, $I_b/j\omega CV_c$ is negligible except in the last term of each equation, where it is multiplied by Q. Let us introduce $\eta \equiv 1/(\omega^2 MC \cos \beta_1 \ell_1)$, $G \equiv R/(\omega M \cos \beta_1 \ell_1)^2$, $Q \equiv \omega L/R$, $\omega_0 \equiv 1/\sqrt{LC}$, and $2\delta_L \equiv 1 - \omega_0^2/\omega^2$, to simplify the equations. Then

$$\frac{V_m}{V_C} \approx \frac{1}{\eta} \left\{ 1 + j\, \alpha_1 \ell_1 \tan \beta_1 \ell_1 + \left[\alpha_1 \ell_1 Z_{01} + j\, \xi \cos^2 \beta_1 \ell_1 \right] \times G \left[1 + j\, 2\delta_L Q + \frac{I_b Q}{\omega C V_c} \right] \right\}. \tag{12}$$

Now notice that if the losses in the coupling line are small ($\alpha_1 \ell_1 << 1$), and if the detuned-short constraint is met ($\xi << 1$), then we have voltage lock between the manifold and cavity, since the ratio is only slightly affected by cavity tuning (δ_L) and beam current I_b. However, the value η can be changed mechanically by rotating the coupling loop so that M varies.

The perturbations in the load current at the manifold are relatively small and Eq. (11) reduces to

$$I_m \approx \frac{1}{\eta} \left\{ + j\, \frac{\tan \beta_1 \ell_1}{Z_{01}} + G \left[1 + j\, 2\delta_L Q + \frac{I_b Q}{\omega C V_c} \right] \right\} V_C \,. \tag{13}$$

The coupling loop inductance L_1 is of the same order as the mutual inductance M, and can not be made zero. For the cavities on our linac, $|\tan \beta_1 \ell_1| = \omega L_1/Z_{01} < 0.2$, and $\cos \beta_1 \ell_1 \approx 1$.

The beam current I_b will have some phase angle with respect to the cavity fields, and so will in general contribute both a real and an imaginary part to be added to $1 + j\, 2\delta_L Q$. We can define G' and δ'_L so that

$$G'(1 + j\, 2\delta'_L Q) = G\left(1 + j\, 2\delta_L Q + \frac{I_b Q}{\omega C V_c}\right) .$$

This is equivalent to saying that the beam loads the cavity and detunes it. Without beam the primed values reduce to the unprimed values. Equation (12) can be rewritten as

$$\frac{V_m}{V_C} = \frac{1}{\eta} \left\{1 + \left[\alpha_1 \ell_1 Z_{01} G' - G' 2\delta'_L Q \xi \cos^2 \beta_1 \ell_1\right] + j \left[G' \xi \cos^2 \beta_1 \ell_1 + \alpha_1 \ell_1 Z_{01} 2\delta' Q G'\right]\right\}. \quad (14)$$

This is analogous to (13), and it is clear that the terms in brackets represent the deviation in amplitude and in phase from perfect voltage lock. Note that by a small adjustment in length of the coupling line, the parameter can make either term in brackets zero at the expense of the other. For a practical coaxial line capable of carrying 1 MW, a typical value of $\alpha_1 \ell_1 \approx 5 \times 10^{-4}$. An error of 1 mm in the adjustment of line length would give $\xi \approx 6 \times 10^{-4}$. We shall assume that with 100% beam loading and a 30-deg synchronous phase angle $I_b Q/\omega C V_c = 1 - j/2$. Let the coupling line have a $Z_{01} = 50$ ohms, and without beam $G = 1/450$ mhos and $2\delta_L Q = -1/2$. With beam loading let $G' = 2/450$ and $2\delta'_L Q = 0$. Without beam Eq. (14) becomes

$$\frac{V_m}{V_C} = \frac{1}{\eta} \left[1 + 0.55 \times 10^{-4} - j\, 0.29 \times 10^{-4}\right],$$

and with beam, Eq. (14) becomes

$$\frac{V_m}{V_C} = \frac{1}{\eta} \left[1 + 1.1 \times 10^{-4} + j\, 0.027 \times 10^{-4}\right].$$

Thus the voltage lock is good to about 1 part in 9000, and the phase lock to about 0.002 deg despite the detuning and the changes due to beam loading. It should be emphasized that it is the fields within one cavity diameter from the coupling loop that are locked this tightly. If the cavity is too long, the fields along its length will fall off from the value near the loop, and this is one reason that it is desirable to have short cavities in a heavily loaded Alvarez linac.[1] This effect can be further reduced by using two or more feed lines from the manifold.

The admittance at the load point on the manifold is the ratio of Eqs. (14) and (13),

$$Y_L = \frac{I_m}{V_m} \approx j \frac{1}{Z_{01}} \tan \beta_1 \ell_1 + G \left(1 + j\, 2\delta_L Q + \frac{I_b Q}{\omega C V_c}\right). \tag{15}$$

The admittance at the load point is different from that at the loop because the self-inductance of the loop requires the coupling line to be shorter than a multiple of $\lambda/2$. The principal effect of the loop is to change the resonant frequency slightly because of the reactive energy in the coupling line. We can define a double-primed G'' and δ''_L to include both beam current and loop inductance,

$$Y_L \equiv G''(1 + j\, 2\delta''_L\, Q),$$

to justify the assumption that the coupling line and the cavity can be represented by this functional form as assumed in Eq. (4).

IV. OTHER MODES IN THE OPERATING PASSBAND

Now that we have approximate equations which explain the manifold properties for the operating frequency, let us study other modes that can be excited on a manifold system. We shall show that the operating frequency in a manifold system lies in the center of a passband, and that the mode separation varies inversely as the length of the system. From the diagonal terms in the matrix Eq. (1), we can define

$$\cosh \gamma_L \ell \equiv \cosh \gamma \ell + (Y_L/2Y_0) \sinh \gamma \ell\ , \tag{16}$$

where $\gamma \equiv \alpha + j\beta$ and $\gamma_L \equiv \alpha_L + \beta_L$ are the propagation constants for the unloaded line and for the loaded section of manifold. Using the approximations from the previous section, we have

$$\cosh \alpha_L \ell \cos \beta_L \ell \approx \cos \beta\ell \times \left(1 + \alpha\ell\ \frac{G}{2Y_0}\right) - \sin \beta\ell \times \left(+\ \frac{G\delta_L Q}{Y_0}\right), \tag{17}$$

$$\sinh \alpha_L \ell \times \sin \beta_L \ell \approx \sin \beta\ell \times \left(\alpha\ell\ + \frac{G}{2Y_0}\right) + \cos \beta\ell \times \left(+\ \frac{G\delta_L Q}{Y_0}\right). \tag{18}$$

Both $\delta_L = (\omega - \omega_0)/\omega$ and $\beta = \omega/v$ are functions of ω, where v is the velocity of propagation on the manifold transmission line. The terms on the right-hand side of the equations are known, and we can obtain β_L and α_L by solving the two equations simultaneously. These parameters define a passband

for a loaded section of manifold. The following approximations are an aid in solving the above equations: In the passband $\cosh \alpha_L \ell \approx 1$ and $\cos \beta_L \ell < 1$, while in the stop band $\cosh \alpha_L \ell > 1$ and $\cos \beta_L \ell \approx 1$. If the losses are small, the approximate half-width of the passband can be found by finding the frequency for which the right-hand side of (C.2) has an absolute value greater than unity.

Then
$$-1 = \left(\cos \frac{\Delta\omega}{\omega_0} \quad n\pi\right) \times \left(1 + \alpha\ell \frac{G}{2Y_0}\right) - \left(\sin \frac{\Delta\omega}{\omega_0} \quad n\pi\right) \times \left(\frac{GQ}{Y_0} \frac{\Delta\omega}{\omega_0}\right)$$

or
$$\frac{\Delta\omega}{\omega_0} = \left[\frac{2 + \alpha\ell \frac{GQ}{2Y_0}}{n\pi\left(\frac{n\pi}{2} + \frac{GQ}{Y_0}\right)}\right]^{1/2} \approx \left[\frac{2\,Y_0}{n\pi GQ}\right]^{1/2}, \tag{19}$$

where $\Delta\omega$ is the half-width of the passband. For our linac the passband is about 800 kHz wide, and it is symmetrical around the operating frequency. There are other passbands near each cavity resonance. We have designed our system so that the nearest cavity resonance lies outside this operating passband, but if another cavity resonance did fall within the passband, it would split the band in two with a narrow stop band between. The new operating passband would be unsymmetrical, with the modes on one side crowded together.

For the remainder of this analysis we consider the loaded manifold to consist of N identical sections so that we can study the modes in the passband. At the operating frequency there is a phase shift of $n\pi$ between load points, and the total phase shift from end to end is $Nn\pi$. The phase shift due to the transmission line and cavity combination between two load points can change as much as $\pm\pi$. The nearest modes on the manifold system occur when the total end-to-end phase shift is an additional $\pm\pi$, or when each cavity has contributed an additional $\pm\pi/N$. This is shown on the ω-β_L curve in Fig. 3. Additional resonances occur when the total end-to-end phase shift is changed by $\pm 2\pi$, $\pm 3\pi$, $\cdots$ $\pm N\pi$. We call this set of resonances the -N mode, $\cdots$, -2 mode, -1 mode, zero mode (operating mode), +1 mode, +2 mode, $\cdots$, +N mode. From our computer study, and also from measurements that we have made on a model manifold, we find that at the ± 1 modes the largest voltage is at the end loads, with very little at the center load; for any mode the distribution of voltage along the load points approximates points on

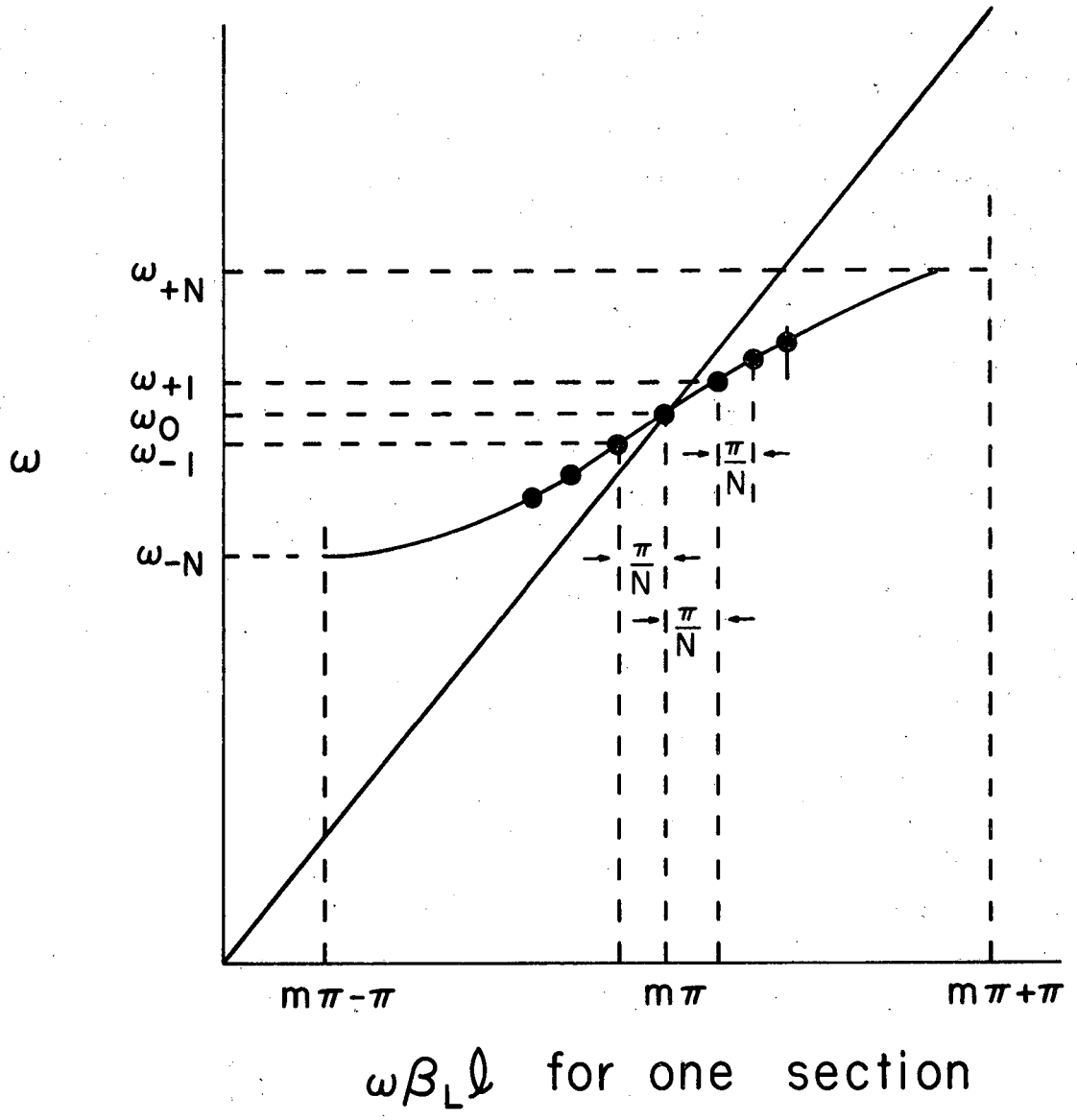

Fig. 3. ω-$B_L\ell$ for one section of the manifold system.

a cosine wave with as many nulls as the number of the mode. It is difficult to excite the ±1 modes by driving near the center of the system, since this is a nodal point for odd-numbered modes. In general, if there is a symmetrical array of M amplifier drive points, the first ±M modes (except the zero mode) tend to be suppressed. This property is a good reason for distributing the drive amplifiers along the length of the manifold instead of at one end. Distributing the amplifiers, so that the power source is near the load, also reduces the perturbation in voltage from one end of the manifold to the other, since the deviation from perfect voltage lock is proportional to the product of power flowing times the length of manifold through which it flows.

The full-scale manifold does not have uniform loads, but fortunately it is not difficult to put data for a nonuniform system into our computer program and calculate the expected resonances. We compared resonant frequencies from the computer, using actual linac parameters, with frequencies obtained from the $\omega - \beta_L$ curve, assuming uniform cavity parameters that were the average of the actual values. In the center region of the passband the distribution of modes agreed closely with the values from the more complicated solution.

The most important modes are those near the operating frequency, and an approximate method of predicting the separation of the nearest modes is very useful. Let us make the approximation that $\cos \alpha_L \ell \approx 1$ in the middle of the passband. Also let us assume that $\beta\ell = n\pi + \delta_1 n\pi$, where $\delta_1 \equiv (\omega_1 - \omega_0)/\omega_1$ is the incremental frequency to the nearest mode. At the nearest mode $\beta_L \ell = n\pi + \pi/N$ for one section. Substituting into Eq. (17) gives

$$\cos \frac{\pi}{N} = 1 + \alpha\ell \frac{G}{2Y_0} + \delta_1 n\pi \left(\omega L_1 Y_0 - \frac{GQ}{Y_0} \delta_1 \right)$$

If $\pi/N < 0.3$ or $N > 10$, then $\cos \pi/N \approx 1 - (\frac{1}{2})(\pi^2/N^2)$, and since for most practical cases $\omega L_1 Y_0 << \frac{GQ}{Y_0}$ and $\alpha\ell \frac{G}{Y_0} << 1$, this equation reduces to

$$1 - \frac{1}{2} \frac{\pi^2}{N^2} \cong 1 - \delta_1^2 n\pi \frac{GQ}{Y_0} ,$$

or

$$\delta_1 = \pm \frac{1}{nN} \left[\frac{n\pi Y_0}{2GQ} \right]^{1/2} . \qquad (20)$$

This equation gives the mode separation near the operating frequency. Notice that since nN is proportional to the length of the whole manifold, this equation shows that the mode separation varies inversely as the first power of the linac length in a manifold system. This is in contrast to a long Alvarez cavity operating on TM_{010} mode without a manifold which has a mode separation that varies as the square of its length.

V. TRANSIENTS

We expect the principal transient effects to be caused by excitation of those modes in the operating passband that are nearest to the operating frequency. In general, the nearer the mode is to the operating frequency, the stronger its response to a sudden change in power level. The response to a given mode is modified, however, by where the power level is changed in the system. For example, when power is fed at the center of the system, the odd-numbered modes tend to be suppressed. Similarly with a symmetrical drive of M amplifiers, the first ±M modes are suppressed (except for the zero mode), and it is the differential change in power level that tends to excite the nearby modes. The transients typically appear as oscillations superimposed on the leading or trailing edge of the rf envelope of the cavity voltage. The amplitudes of the oscillation are frequently larger on the trailing edge, since power can be interrupted faster than it can be turned on at the beginning of the pulse. Several frequencies can be present in the oscillations, and these will be in different proportions in the various load cavities.

To find an analytic solution for the transient problem, we shall make some simplifying assumptions that will allow us to solve a simpler problem. The functional form of the solution gives us insight into the more difficult problem, which is best solved on a computer. We assume the amplifier to be located at one end of the system so that any pair of modes may be excited. The impedance of the manifold at the amplifier location is assumed to consist of the zero mode and two modes symmetrically spaced in frequency above and below the zero mode. These normally would be the ±1 modes, and they would be symmetrically spaced if the manifold were properly tuned. Figure 4 shows a complex frequency plot of the impedance with zeros introduced symmetrically as they seem to be in the computer solutions for resonance. For ease of calculation, we will assume the Q of all the modes to be the same. This analysis neglects other nearby modes which also contribute

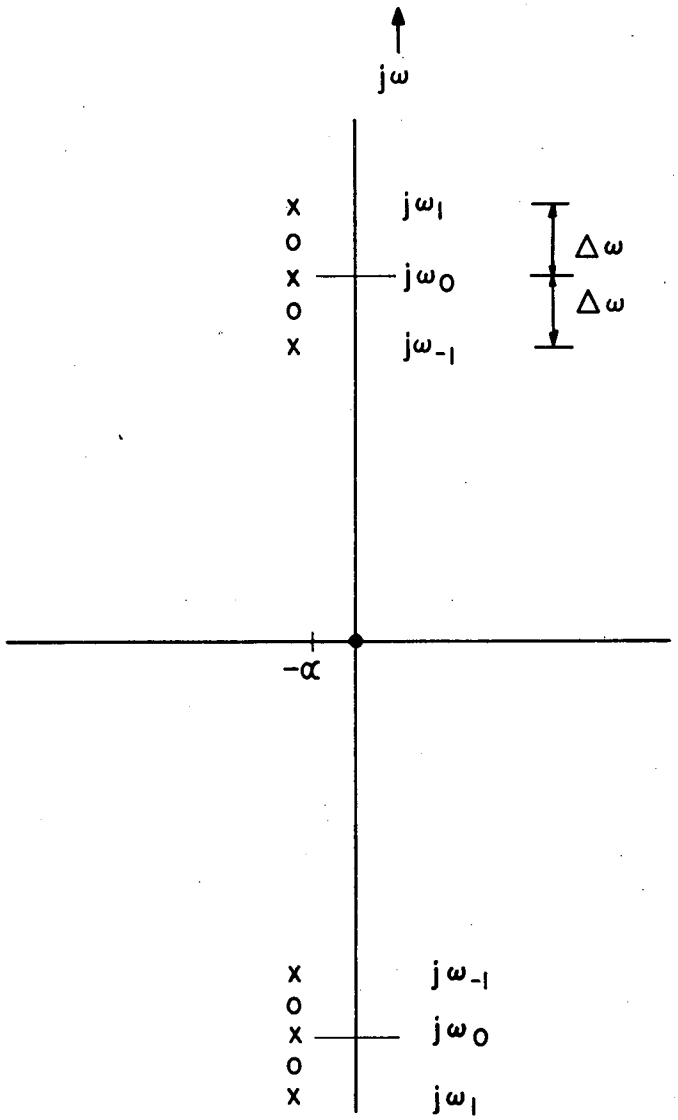

Fig. 4. Complex frequency plot of the impedance.

beat frequencies. Several pairs of modes can be included, but the calculation gets quite involved, and it is not a bad approximation to superpose the transients calculated for each pair of modes one at a time.

The problem becomes much simpler if we can use a simple driving function, so that the driving current from the amplifier is chosen to be

$$i(t) = i_0(1 - e^{-kt}) \sin \omega_0 t \, .$$

This assumes that if the modulator level is changed suddenly, the amplifier responds in a time which is short with respect to the cavity time constant, but is still an exponential function. The Laplace transform of the function is

$$i(s) = i_0 \left[\frac{\omega_0}{S^2+\omega_0^2} - \frac{\omega_0}{(S+k)^2+\omega_0^2} \right] ;$$

then

$$V(s) = i(s) \cdot Z(s) \, ,$$

where the poles and zeros of Z(s) are shown in Fig. 4 . It is not difficult to get the inverse Laplace transform of V(s) as a sum of exponential terms which can be reduced to sinusoidal functions by suitable regrouping. The solution for V(t) is proportional to

$$V(t) \propto \left\{ \frac{1}{\alpha} (1-e^{-\alpha t}) - \frac{1}{k-\alpha} e^{-\alpha t} + \frac{1}{k-\alpha} \left[\frac{4(k-\alpha)^2 + \overline{\Delta\omega}^2}{(k-\alpha)^2 + \overline{\Delta\omega}^2} \right] e^{-kt} \right. \qquad (21)$$

$$\left. + e^{-\alpha t} \left[\frac{6}{\Delta\omega} - \frac{6\Delta\omega}{(k-\alpha)^2 + \overline{\Delta\omega}^2} \right] \sin\omega t - e^{-\alpha t} \left[\frac{6(k-\alpha)}{(k-\alpha)^2 + \overline{\Delta\omega}^2} \right] \cos \Delta\omega t \right\} \sin \omega_0 t \, ,$$

where $\alpha = \omega/2Q$ is the time constant of the system, and where the various coefficients in brackets are related to the spacing between the zeros and the poles. The value $\Delta\omega$ is the difference in frequency between the operating frequency and the adjacent modes. There are no quadrature terms proportional to $\cos \omega_0 t$ because of the symmetry of ω_{+1} and ω_{-1} . A desirable condition would be for $\Delta\omega >> k >> \alpha$; Eq. (21) then reduces to

$$V(t) \propto \left\{ \frac{1}{\alpha} (1 - e^{-\alpha t}) - \frac{1}{k} (e^{-\alpha t} - e^{-kt}) - \frac{6k}{(\Delta\omega)^2} e^{-\alpha t} \cos \Delta\omega t \right\} \sin \omega_0 t \, .$$

The first two terms are the normal response of a cavity to a sudden change, and the third term is the effect of the nearby symmetrical modes. From this equation it is obvious that the faster we try to drive the system (the larger k becomes), the larger the beat-frequency term will be.

In a linac with a large amount of beam loading, one needs to regulate the power being fed into the manifold during the pulse, and this requires an amplifier-modulator system with a high frequency response. The value of k is related to the modulator frequency response, and if k approaches $\Delta\omega$, the regulator can become unstable, and the beat-frequency terms become continuous oscillations. This problem exists for other systems as well as for the manifold system.

VI. DESCRIPTION OF MODEL MANIFOLD SYSTEM

The model manifold system shown in Fig. 5 consists of three parts: a one-tenth-length manifold, six resonant-cavity loads with coupling lines, and the amplifier drive system. The rf manifold is made of 18 accurately machine sections of coaxial line that are each 5.7 cm in diameter and 75 cm long. The characteristic impedance of the coaxial line is 35.5 Ω. The inner conductor is supported on a continuous Styrofoam insulator, and each section is electrically connected to the next by rf spring fingers. A threaded steel rod through the center pulls all 18 sections of outer conductor together. The two sections are short-circuited at the outer ends, making the manifold 18 half-wavelengths long at 195.770 MHz when the manifold is at 17°C. The overall length of nearly 50 ft has the same attenuation from end to end as the full-scale manifold we have been considering. In the middle of each section there is a provision to insert a fitting that allows electrical connection to the inner conductor through a GR 848 connector. These connections are the mesh points of the manifold, and they are at the voltage maximum points of the unloaded manifold.

The resonant-cavity loads are sections of a coaxial line which are foreshortened by a gap that can be adjusted with a micrometer head. The outer diameter is 6 in. and the cavity has an unloaded Q of approximately 5000. Electrically the cavity is a quarter wave long, and near the short-circuited end are two coupling loops which have been rotated to give respectively 50 Ω and 350 Ω input impedance at resonance. Since the shunt impedance of the cavities is about 500 kΩ, this is equivalent to a turns ratio

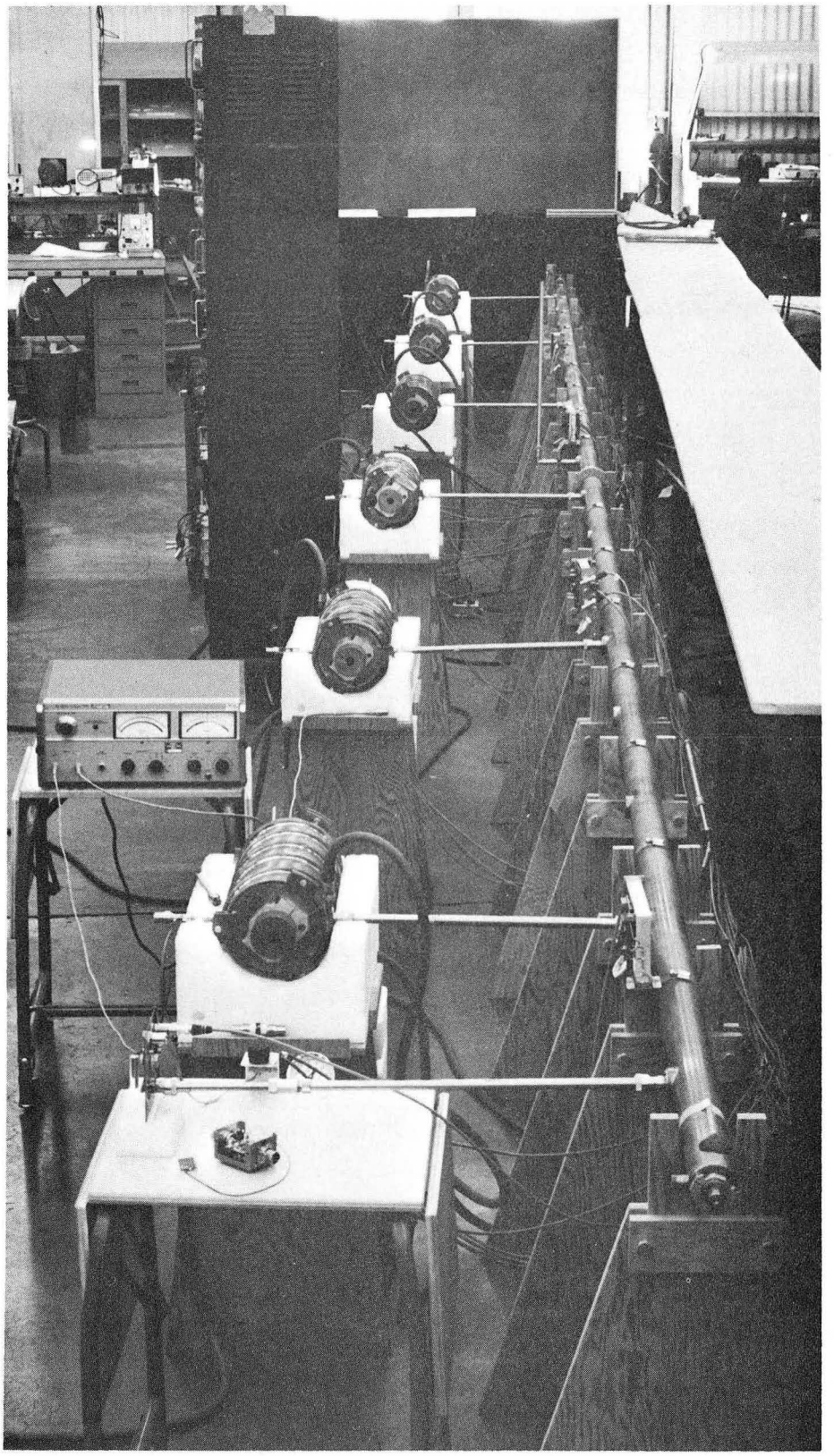

Fig. 5. Model manifold system. ZN-5815

of 100 and 38 respectively between the gap voltage and the loops. The micrometer allows a fine adjustment of the unloaded resonant frequency of 575 kHz with ±50 mils of motion.

The cavities are normally adjusted to have the same resonant frequency as the unloaded manifold. The next higher cavity resonance is at 585 MHz, and there are about 23 additional resonances below 2000 MHz. Each cavity has six turns of 1/4-in. copper water tubing soldered to its outer diameter, and the cavities are mounted in thick Styrofoam jackets so that they will come to the temperature of the circulating water. The six water circuits are connected in series, so that all the cavities stay at the same temperature. The cavities are connected to the manifold by an adjustable GR 50-Ω coaxial line. During the process of adjusting the coupling loops, the length from the cavity to the detuned-short position on the coupling line is determined. When the cavity is connected to the manifold the coupling-line length is adjusted so that the detuned-short position falls at the center of the manifold.

Figure 6 is a closer view of one end of the system, showing a cavity load and an amplifier connected to the manifold. The drive amplifiers are transistorized and are built on printed-circuit boards. The drive-amplifier board has two class-C radio-frequency stages with strip-line tank circuits. There is also a modulator with a closed-loop regulator, so that the supply voltage to the rf amplifier may be controlled in time and amplitude by a low-level pulse. The low-level rf stage is furnished with a continuous-wave drive voltage of about 1 V rms at the desired rf frequency, and the bandwidth of the drive amplifier is about 5 MHz.

We postulate that the system is ideally tuned (a) when it is driven at the resonant frequency of the unloaded manifold; (b) when the length of coupling line is such that the detuned-short position on the line is connected to the mesh point on the manifold, and (c) when the cavity is tuned to minimize the reactive energy exchanged between the cavity and the rest of the system. This is most easily accomplished on the model by unloading the manifold and tuning the drive frequency for resonance; then the cavities are added (with the premeasured line length) one at a time. Each cavity is retuned to bring the system to resonance before the next is added.

The amplifiers are connected to the system in one of two ways. When going through the tuning-up procedure described above, the amplifier drives

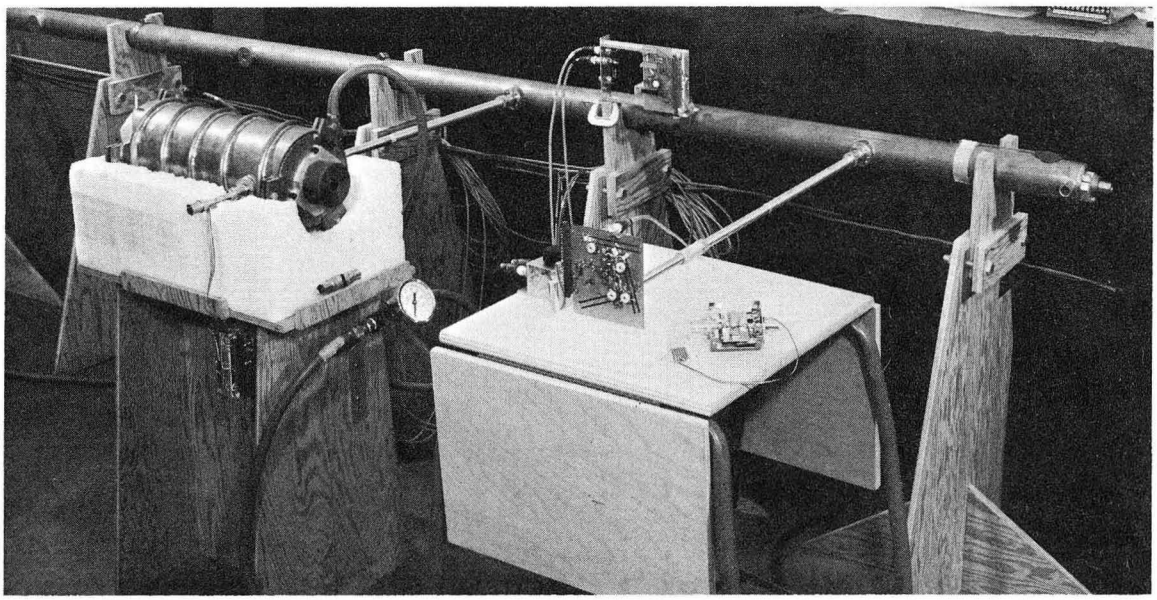

ZN-5814

Fig. 6. One end of model manifold system, showing cavity load and amplifier connected to manifold.

a small loosely coupled loop at one end, and a similar loosely coupled loop at the other end is connected to a 661 sampling scope to monitor the resonances. When the system is correctly adjusted, the amplifier is connected to a mesh point through a half-wave-length coupling line. When the system is pulsed, the rf envelope at several points is monitored by crystal detectors. By observing on the scope the pulse envelope at the amplifier tank circuit and at a cavity simultaneously, one can easily adjust the amplifier coupling line for the tightest coupling.

VII. EXPERIMENTAL RESULTS

We shall discuss several experiments that were designed to check the amplitude and phase lock when the cavity loads were detuned by an excessive amount to make the deviations easier to measure. In the first experiments data were taken with a Hewlett-Packard Vector Voltmeter and recorded directly on an X-Y recorder. These actual experimental graphs are reproduced in Fig. 7 through 9. In each experiment the manifold system was tuned as close to the ideal condition as possible. Then as the drive frequency was swept through the operating frequency, graphs were made of the voltage in two adjacent cavities and of the phase between them. These graphs are labeled Case 1. The amplitudes of the voltage in the two cavities are very nearly the same in the frequency range near resonance, and the recordings look almost like a single pen line. The phase difference between cavities is 180 deg at resonance because the adjacent cavities are separated by $3\lambda/2$ on the manifold. In the first experiment (Fig. 7), Cavity 3 was detuned + 50 mils by its micrometer. This corresponds to detuning the unloaded cavity by 575 kHz or 11 Q-widths. Notice that this detunes the system by about 125 kHz, since most of the energy is stored in the other cavities.

The experimentally determined unloaded Q for the cavities is 3770. Measurements on the coupling line and loop indicate that the equivalent $\alpha_1 \ell_1 = 0.00475$. The equivalent load resistance of the cavities was adjusted (by rotating the loops) to be $R_L = 345$ ohms. To calculate the deviation from perfect amplitude and phase lock between the two cavities, we first calculate the voltage ratio between the detuned Cavity 3 and the manifold from Eq. (14) (see Fig. 10):

$$\frac{V_{m3}}{V_{C3}} = \frac{1}{N}\left\{1 + \left[\alpha_1 \ell_1 Z_{01} G - 2\delta_L Q G \xi_3 \cos^2 \beta_1 \ell_1\right] + j\left[G\xi_3 \cos^2 \beta_1 \ell_1 + \alpha_1 \ell_1 Z_{01} G 2\delta_L Q\right]\right.$$

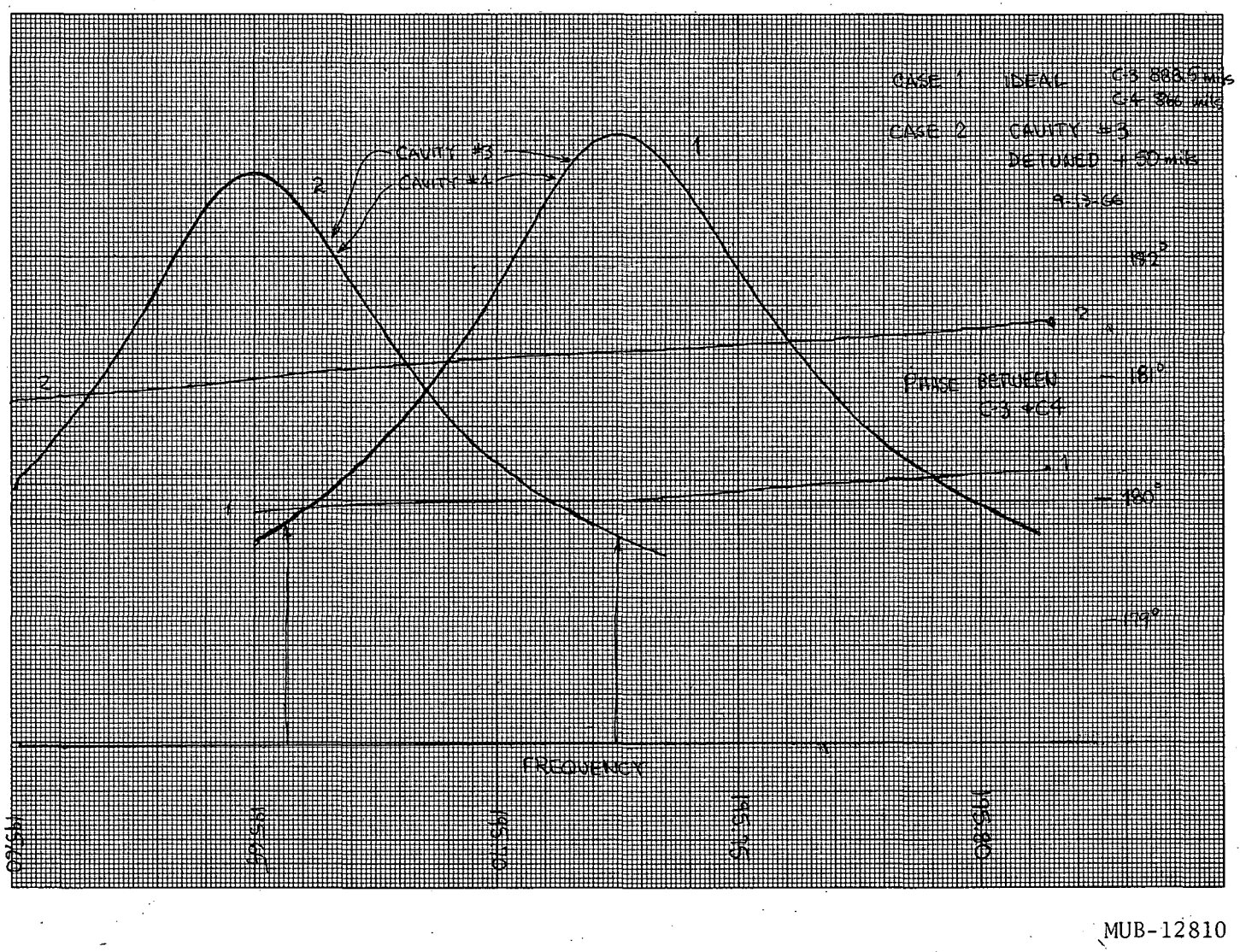

MUB-12810

Fig. 7. Graph of experiment No. 1 with model manifold system.

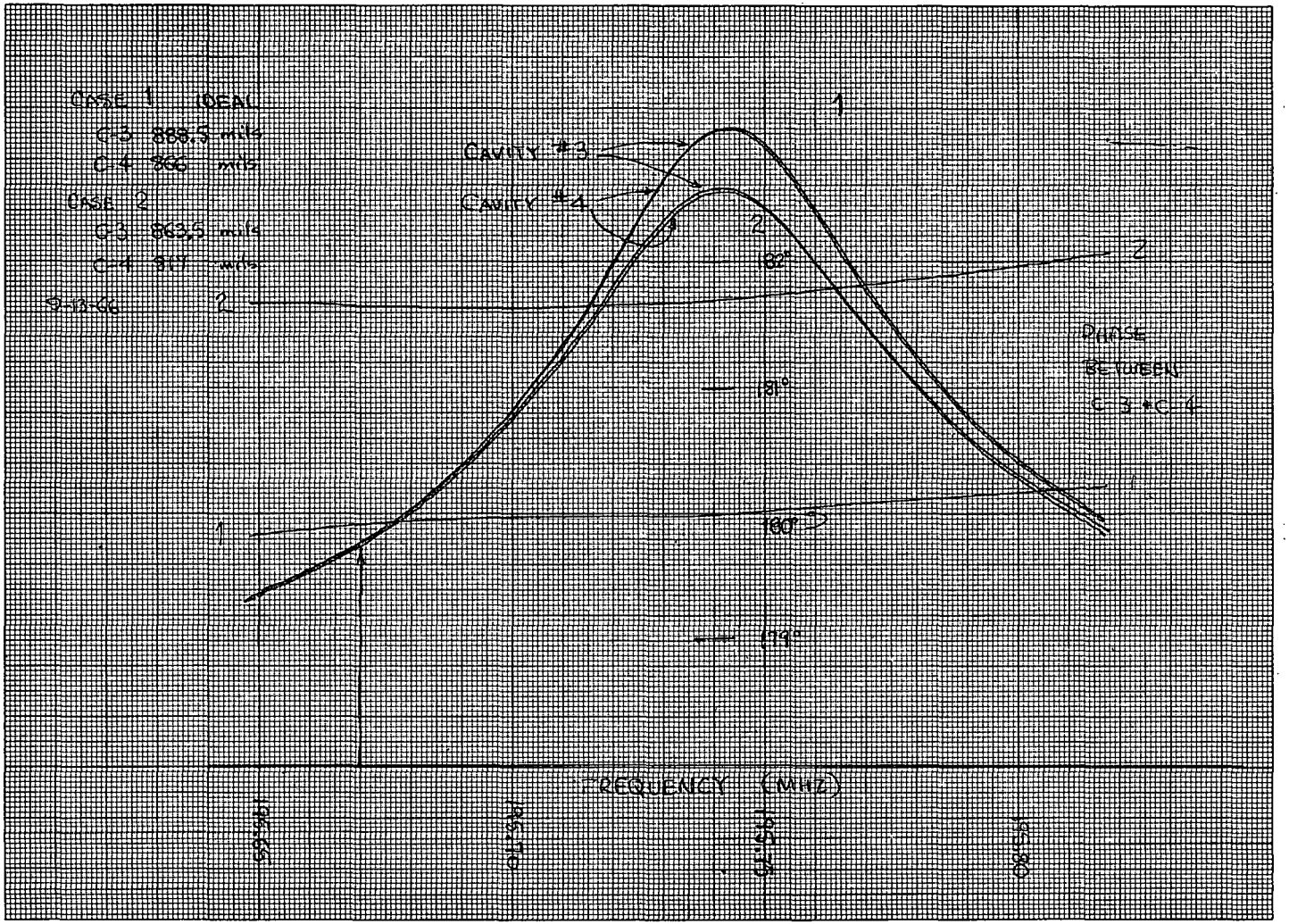

MUB-12807

Fig. 8. Graph of experiment No. 2 with model manifold system.

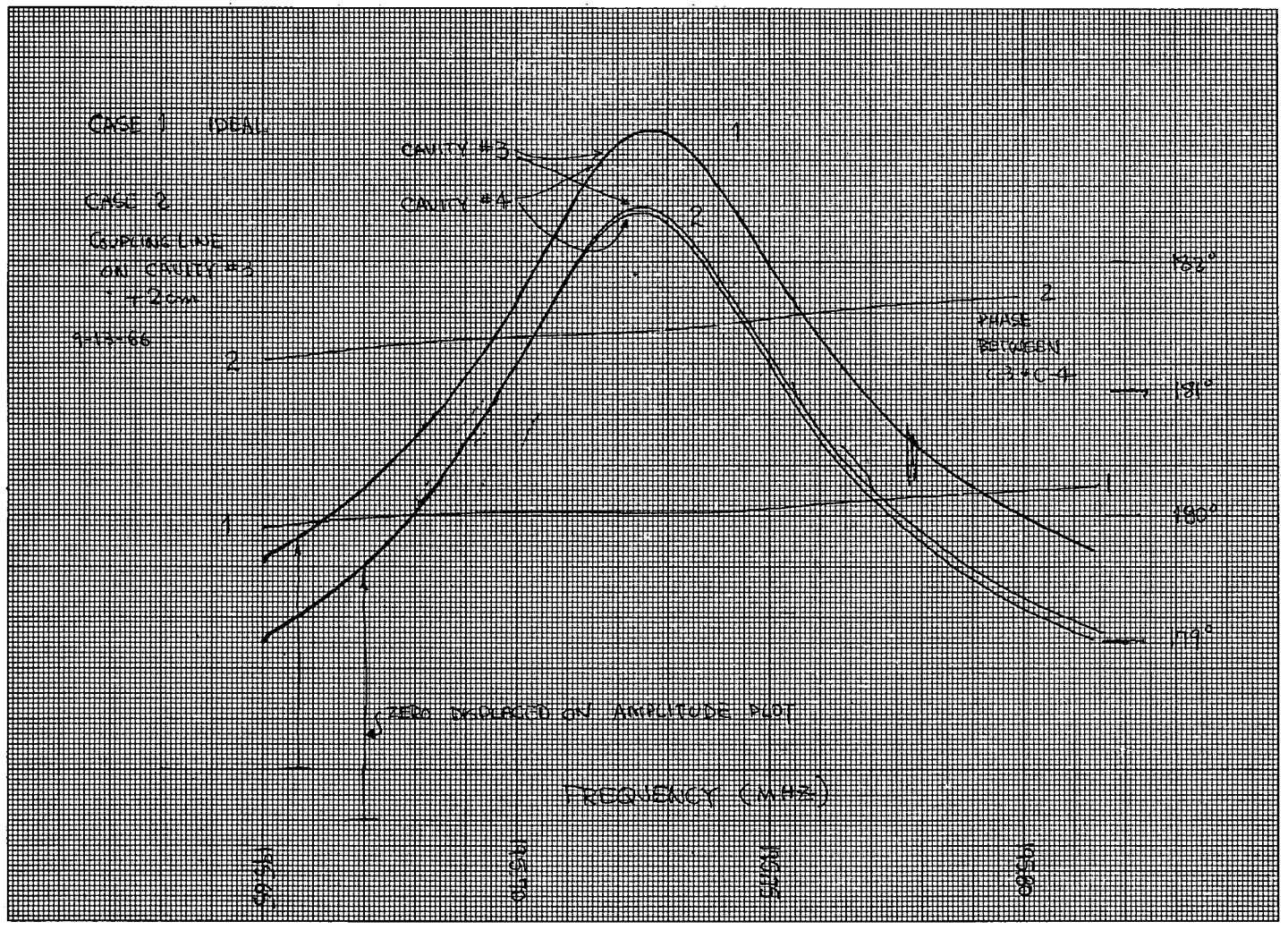

MUB-12808

Fig. 9. Graph of experiment No. 3 with model manifold system.

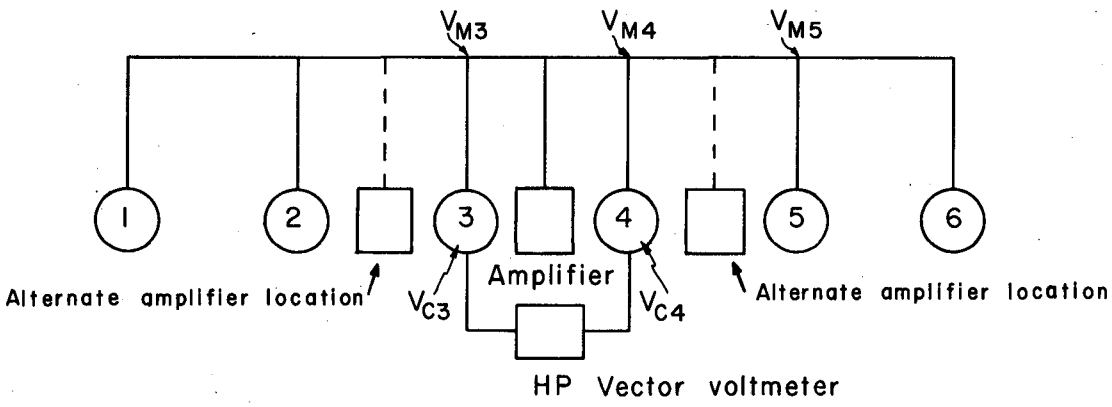

Fig. 10. Block diagram of the model manifold.

Now $\ell_1 = 52.9$ cm, and $\beta_1 \ell_1 = 124.5$ deg, or $\cos^2 \beta_1 \ell_1 = 0.32$. The measured value of $G = 1/345 = 0.0029$. By the correct adjustment of coupling line lengths we should get $\xi = 0$. Actually the coupling line length for a given cavity was adjusted in small increments as the micrometer on the cavity was rocked back and forth through resonance. An oscilloscope display of the six cavity voltages was observed, and the length ℓ_1 was assumed correct when the voltage in the cavity being adjusted deviated by a minimum amount from the other cavities as the tuning passed through resonance. After the six coupling lines had been successively worked through several times, ℓ_1 for each cavity was probably within 0.5 mm of the ideal length. The coupling lines were adjustable GR 50-Ω lines with $\alpha_1 \ell_1 Z_{01} = 0.237\,\Omega$. Substituting these values into Eq. (14) gives, for $\delta_L Q = 11$,

$$\frac{V_{m3}}{V_{C3}} = \frac{1}{N}\left\{1 + 0.689\times10^{-3} - 0.022\,\xi_3 + j\,(0.001\,\xi_3 + 15.2\times10^{-3})\right\}.$$

The voltage ratio between Cavity 4 and the manifold should be the same except that $\delta_L = 0$ for this cavity. Then

$$\frac{V_{m4}}{V_{C4}} = \frac{1}{N}\left\{1 + 0.689\times10^{-3} + j\,0.001\,\xi_4\right\}.$$

Next we must include the voltage ratio along the manifold from Eq. (6). The calculated value for α on the model manifold is 7.77×10^{-4}, $\ell = 2.25$ meters, and $Y_0 = 1/35.5\,\Omega$, so that $\alpha\ell/Y_0 = 0.062\,\Omega$. There are two more tuned cavities beyond Cavity 3, making $I_n/V_n = 2G$. By choosing the operating frequency carefully, we have made $\delta_0 = 0$, and we get

$$\frac{V_{m3}}{V_{m4}} = 1 + 0.54\times10^{-3} + j\,1.8\times10^{-3}.$$

Then the calculated voltage ratio between the two cavities should be

$$\frac{V_{C4}}{V_{C5}} = \frac{\frac{1}{N}\left[1 + 0.689\times10^{-3} - 0.022\,\xi_3 + j\,(0.001\,\xi_3 + 15.2\times10^{-3})\right]}{\frac{1}{N}\left[1 + 0.689\times10^{-3} - j\,0.001\,\xi_4\right]}$$

$$\times\left[1 + 0.54\times10^{-3} + j\,1.8\times10^{-3}\right]$$

$$\approx 1 + 0.54\times10^{-3} - 0.022\,\xi_3 + j\left[17\times10^{-3} + 0.001\,(\xi_3 - \xi_4)\right].$$

If the ξ's were zero, the amplitude deviation would be 0.54×10^{-3} and the phase deviation would be 0.97 deg. However, adjusting for the minimum is

critical, and an error of 0.5 mm in ℓ_1 could result in $\xi = 0.18\Omega$, which would make $0.022\ \xi_3 = 4\times10^{-3}$ and $0.001\ \xi_3 = 0.2\times10^{-3}$ in the above equation. This would not affect the phase much, but it could make an order-of-magnitude change in the amplitude deviation. The measured amplitude deviation, from Fig. (7) is less than 1/4 division out of 124, or less than 2×10^{-3}, and the measured change in phase is 1.2 deg.

	Deviation	
	Amplitude	Phase (deg)
Measured	$<2\times10^{-3}$	1.2
Calculated	0.54×10^{-3} minimum	0.97

The second experiment consisted of detuning Cavity 3 by +50 mils, and then detuning Cavity 4 in the other direction to bring the system resonance back to the original operating frequency. Figure 8 shows the correctly tuned situation in Case 1, and both cavities detuned in opposite directions in Case 2. With both cavities detuned, we calculate

$$\frac{V_{C4}}{V_{C3}} \approx 1 + 0.54\times10^{-3} - 0.022\ (\xi_3 - \xi_4) + j\ 32.2\times10^{-3}\ ,$$

which corresponds to an amplitude deviation of 0.54×10^{-3} and a phase deviation of 1.85 deg. From Fig. 8, we see an amplitude deviation of about 1/2 division out of 114, or 4.4×10^{-3}, and a change in phase of 1.65 deg.

	Deviation	
	Amplitude	Phase (deg)
Measured	4.4×10^{-3}	1.65
Calculated	0.54×10^{-3}	1.85

Our measuring equipment had a sensitivity of about one part in a thousand for amplitude deviation, and about 0.1 deg in phase. Our ability to adjust ξ to a minimum value is related to the amplitude sensitivity. The next two experiments were designed to perturb the amplitude lock by many times the sensitivity of the measuring instruments, so that we could compare the calculated and measured values.

In the third experiment the coupling line on Cavity 3 was increased in length by 2 cm. For this condition

$$\xi_s = \omega L_1 - Z_{01} \tan \beta_1 \ell_1 = 7.2\Omega .$$

The admittance of the load is given by Eq. (15):

$$Y_L = G + j \left(2\delta_L Q - \frac{1}{Z_{01}} \tan \beta_1 \ell_1\right) ,$$

and since $\beta_1 \ell_1$ changes from 124.5 to 129 deg, increasing the coupling line length is equivalent to detuning Cavity 3 slightly, or so that $2\delta_L QG = - 0.0029$,

$$\frac{V_{m3}}{V_{c3}} = \frac{1}{N} \left\{1 + 21.6\times10^{-3} + j\ 20.9\times10^{-3}\right\} .$$

The errors in other ξ's are neglected. Then the ratio of cavity voltages is calculated to be

$$\frac{V_{c4}}{V_{c3}} \approx 1 + 21.4\times10^{-3} + j\ 22.7\times10^{-3} .$$

This corresponds to an amplitude deviation of 0.021 and a phase deviation of 1.3 deg. From Fig. 9 we see that the measured amplitude deviation is about 1.5 divisions out of 120 or about 0.0125, and the measured phase deviation is 1.23 deg.

	Deviation	
	Amplitude	Phase (deg)
Measured	0.0125	1.23
Calculated	0.021	1.3

In the fourth experiment we held the frequency constant and plotted the voltage in two cavities and the phase between them when Cavity 5 had its coupling line 1 cm too long, and was also detuned. The graph of these values is shown in Fig. 11. It is apparent from this figure that either ξ_5 or ξ_4 was not zero for the control case, because V_{C4} and V_{C5} separate as Cavity 5 is detuned. Increasing the coupling line length on Cavity 5 caused the voltages to separate farther. The calculated ratio for the micrometer

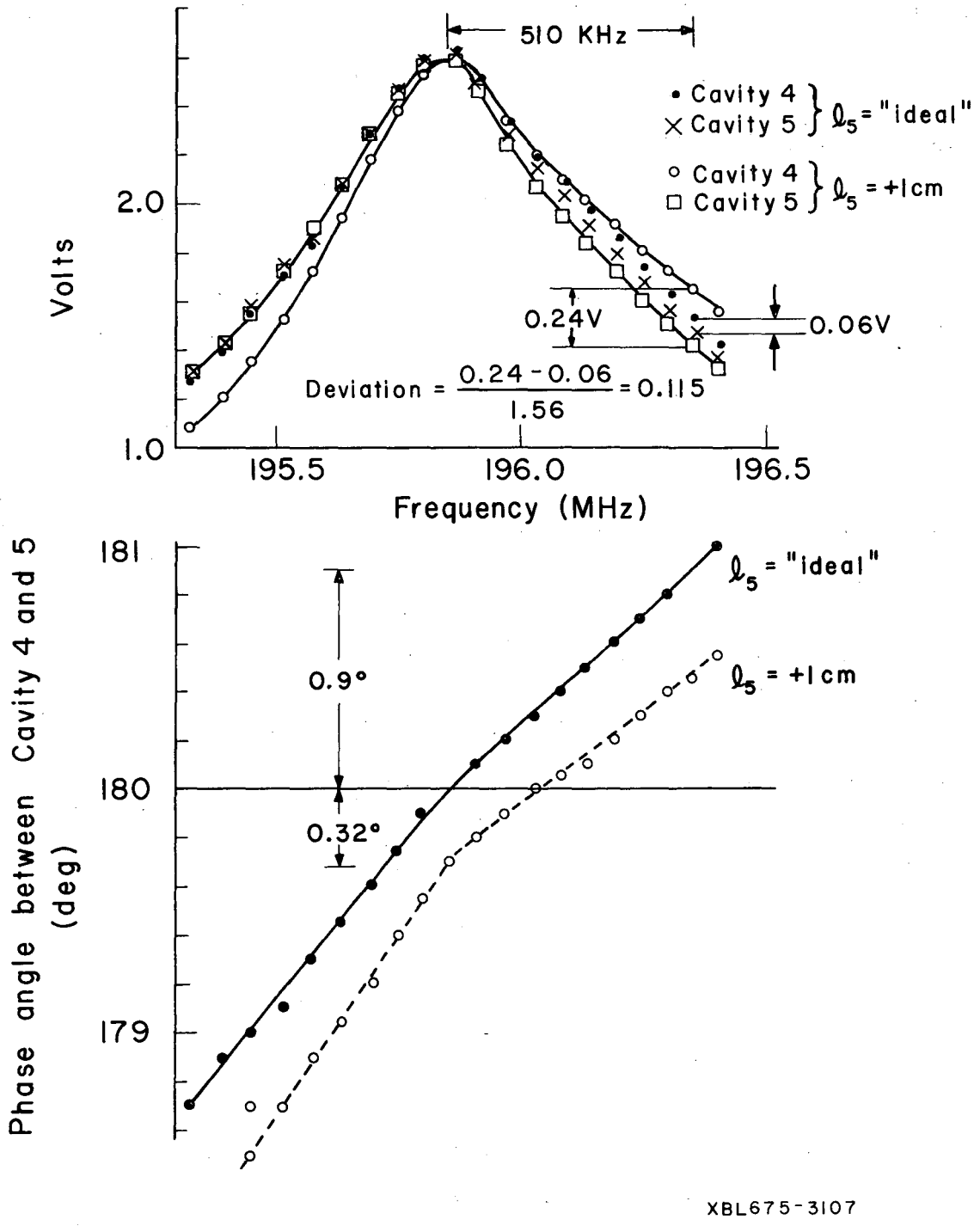

Fig. 11. Graph of experiment 4 with manifold system.

setting of 780 mils is

$$\frac{V_{C4}}{V_{C3}} = 1 + (0.658\times10^{-3} + 0.118) + j\,(5.77\times10^{-3} + j\,13.4\times10^{-3}) .$$

This corresponds to an amplitude deviation of 0.119. The phase deviation will be broken into two parts. The $\xi G = 5.77\times10^{-3}$ corresponds to a phase change of 0.33 deg due to increasing the coupling line length, and $\alpha_1 \ell_1 Z_{01} 2\delta_L QG = 13.4\times10^{-3}$ corresponds to 0.77 deg change in phase due to detuning. This may also be thought of as the slope of the phase curve with respect to detuning. The corresponding measured changes in deviation are shown in the table below.

	Amplitude deviation	Phase jump due to ±1 cm (deg)	Slope of phase curve (deg)
Measured		0.32	0.9
Calculated	0.119	0.33	0.77

We were able to sweep the drive frequency over a 5-MHz range, and we obtained the response of the system for the adjacent modes. Figure 12 shows a typical recording for the voltage in Cavity 5. In order to preserve the linearity on the graph paper, it was necessary to sweep the system several times around a new center frequency, and to step the pen on the graph paper. This accounts for the slight mismatch along the curve at several places. Calculated values obtained from the simple theory in Section IV are plotted on the curve to show that the agreement is very good for the modes adjacent to the operating mode.

Pulsed Operation

Because the Q of our model is about one tenth that of the full-scale system, the rise times are of the order of 10 μsec rather than 100 μsec for the full-scale case. Figure 13 shows the rf envelope of the voltage in Cavities 3 and 6 and the amplifier with rf level being regulated. The amplifier is tightly coupled to the system, so that the amplifier voltage rises at the same rate as that of the cavity. The principal difference between the various voltages is in the phase and amplitude of the superimposed transient

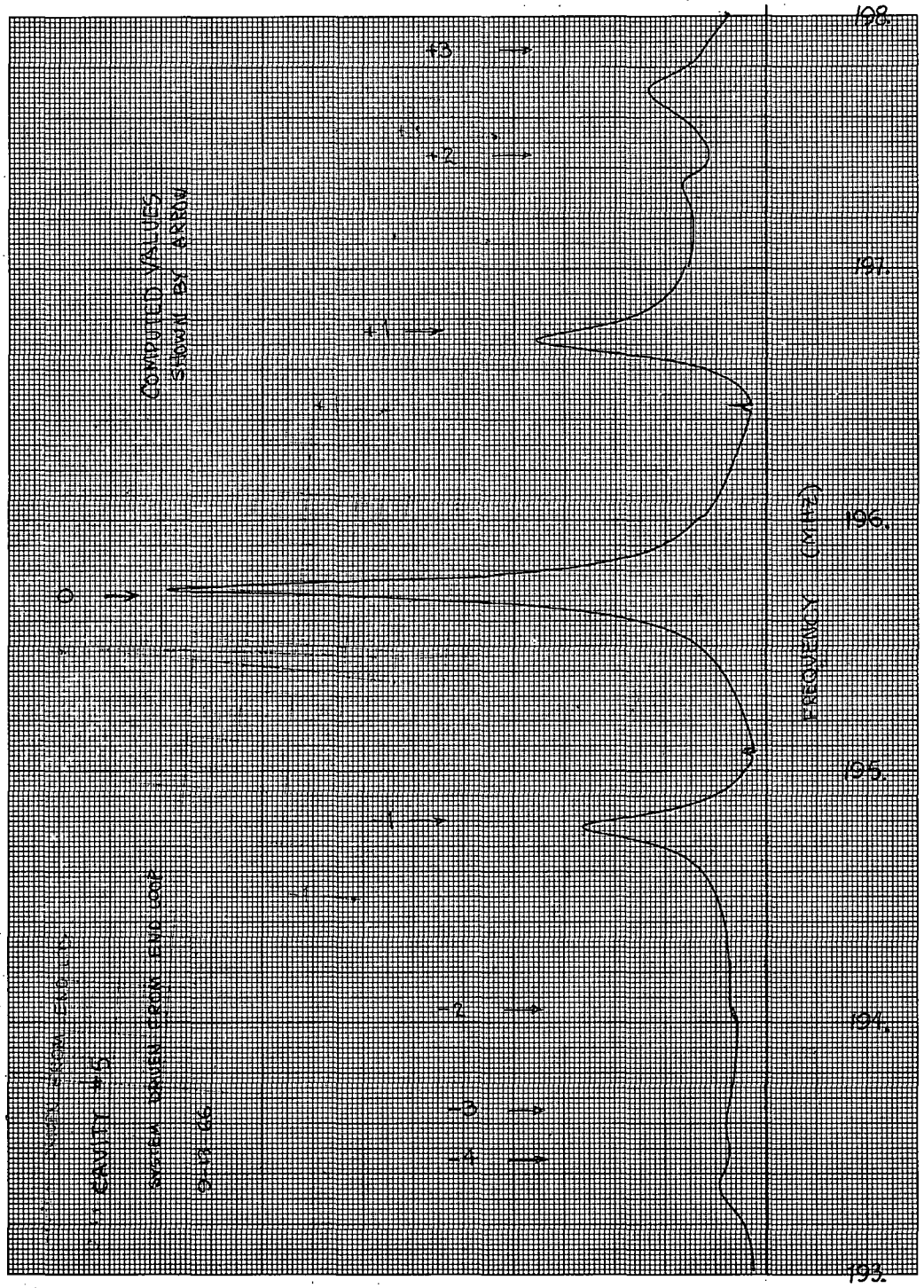

Fig. 12. Adjacent modes on the model manifold.

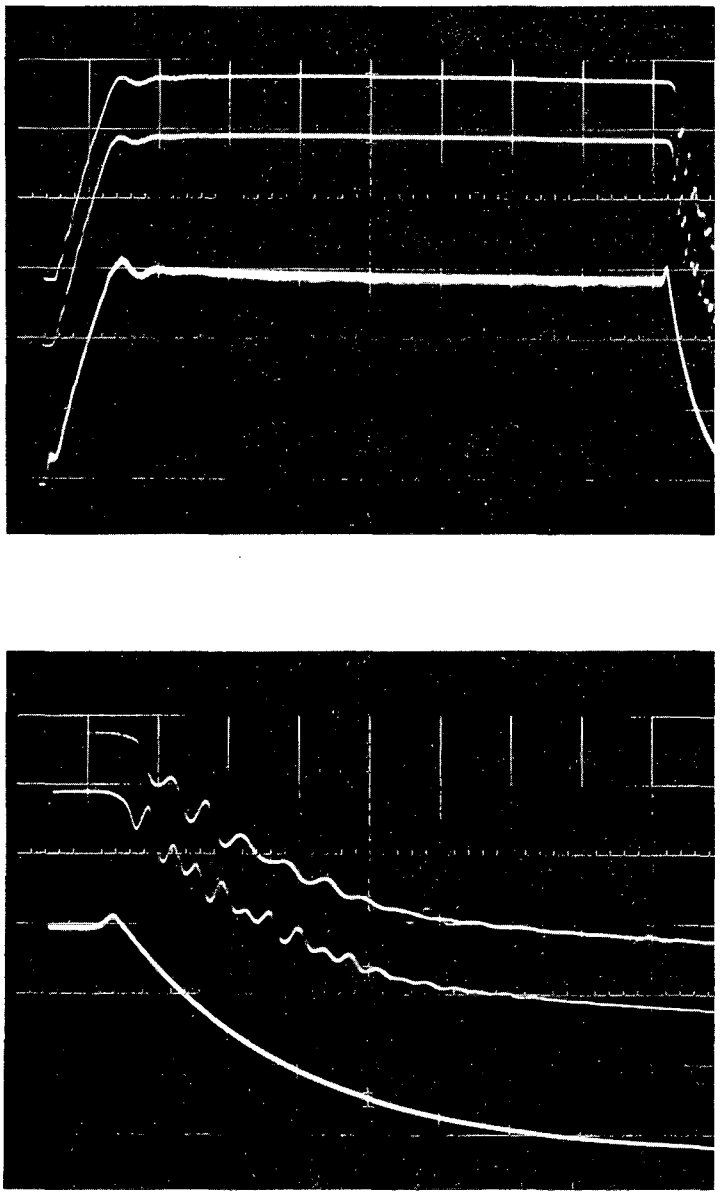

ZN-5809

Fig. 13. (upper) rf Envelope with servo on (5 μsec/cm); (lower) magnification of trailing edge of pulse (1 μsec/cm).

top: Cavity No. 3 voltage.
middle: Cavity No. 6 voltage.
bottom: Amplifier voltage.

during the rise and fall time. The modulator voltage has a ripple that tends to cancel the ripple on the amplifier output. In this case there is some overshoot on the front end of the pulse. The lower figure shows the trailing edge in more detail. The amplifier can interrupt the flow of power more rapidly than it can start power flowing; therefore the transients are excited more strongly. The principal frequency in the falling waveform is about 2 MHz in Cavity 3 and about 3.3 MHz in Cavity 6. This corresponds to the ±2 modes and the ±3 modes, respectively. Since the amplifier is located near the center of the system, it does not tend to excite the ±1 modes. The period of the overshoot on the front end of the pulse corresponds to the bandwidth of the servo amplifier. This was made less than the frequency difference between the operating frequency and the nearest modes in an effort to avoid exciting these modes. In Fig. 14 the bandwidth is large enough to cause continuous oscillation at a frequency which is the same as that excited by the transients.

The transients can be generated either by changes in power from the drive amplifier, or by changes in power absorbed by the load. We were able to change the load in one of the cavities during pulsed operation by putting a microwave planar triode across the gap in the cavity. The anode was connected to one side of the gap, and the grid to the other side. The bias level between grid and cathode was changed during the pulse to bring the triode out of the cutoff region. Since the anode voltage was about equal to the rf voltage across the gap, the electron current flowing across the gap had a 200-MHz component that was in phase with the fields. This simulated beam loading in one cavity lowered the level of the rf voltage in all cavities by an equal amount, just as having an amplifier at one location brings all the cavities to the same level. The beam-loading transient also caused oscillations to be superimposed on the leading and trailing edges of the beam-loading pulse, and it would be difficult to tell by observing the rf envelope of the cavity voltage which transients were due to changes in amplifier level, and which were due to changes in load. Figure 15 shows the rf envelope in one cavity with beam loading in another cavity.

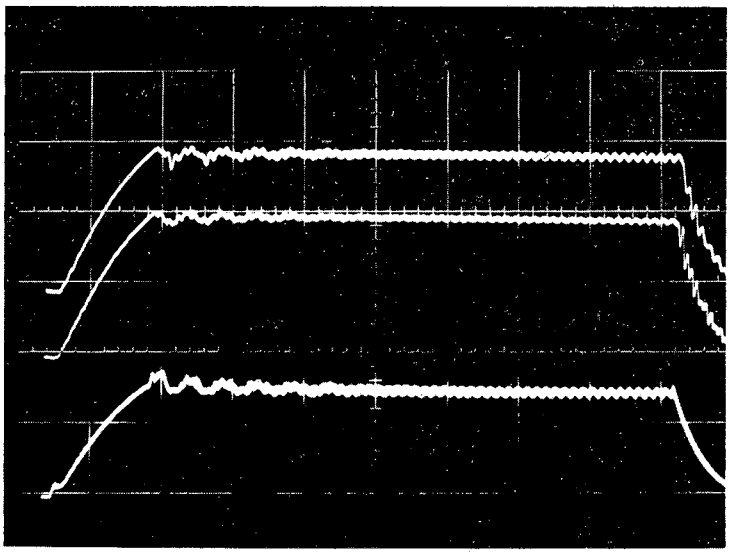

ZN-5812

Fig. 14. rf Envelopes with higher gain and more bandwidth.
top Cavity No. 3 voltage.
middle: Cavity No. 6 voltage.
bottom: Amplifier voltage; 5 μsec/cm.

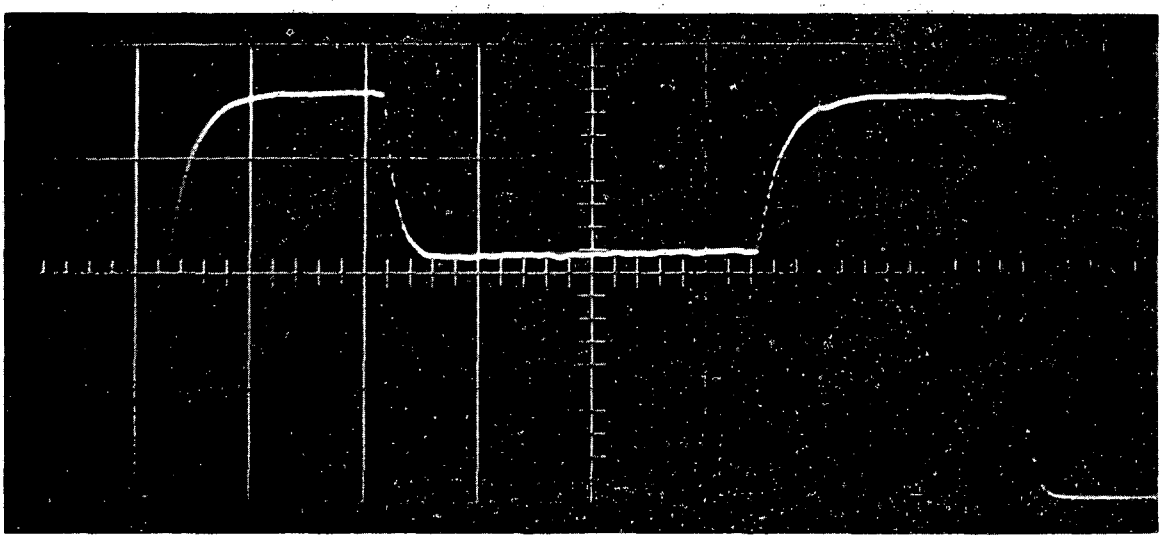

XBB 675-2956

Fig. 15. rf Envelope with beam loading in Cavity No. 3 (30 μsec/cm).

VIII. COMPUTER RESULTS

A full-scale system is much too complicated to analyze without the use of a computer, and we will briefly describe the computer program and show the results for two problems. The computer program starts at a short circuit at the beginning of a manifold with an initial condition that will cause a voltage maximum to occur a quarter wavelength away from the short circuit. This voltage maximum is 30 kV in the two examples which follow. Data are submitted in the form of an IBM card for each element of the system. An integer in the first column identifies the element as a section of manifold transmission line, a coupling line and cavity load, or an amplifier. The cards for the manifold sections specify the length (in meters) of the section. The characteristic impedance and attenuation are specified in separate cards along with frequency and other parameters. The load cards specify the power loss in the walls of the cavity, the Q of the cavity, the resonant frequency of the cavity, and also the energy gain of the cavity. The energy gain is used to calculate beam losses due to a beam of a given current and phase angle which is specified in one of the control cards. The load card also specifies the length of the coupling line. The characteristic impedance and attenuation of the coupling lines are assumed to be the same and are specified on one of the control cards. An amplifier card specifies only the relative power of a particular amplifier.

The identifying number on the element cards causes the computer to calculate the values for the particular type of scattering matrix that is appropriate, and it then calculates the forward and backward voltage wave on the other side of the element. From these it calculates and prints the magnitude and phase of the voltage on the manifold, the standing wave ratio in the manifold, and the power flow in the manifold. If the element is a transmission line it calculates the value of the maximum voltage in the section, and the distance to the maximum. If the element is a load or amplifier, it calculates the power leaving or entering the manifold. It also calculates the magnitude and phase of the voltage across the cavity gap. Figure 16 shows a typical table of elements for the full-scale 200-MeV linac. The first column is the number of the element; the second is the identifying integer (1 = cavity load, 2 = amplifier, 3 = transmission line). The next four columns are load parameters--the copper loss in watts, the Q, the resonant frequency of the cavity

	64						
1	3	-0.	-0.	-0.	-0.	3.72303E-01	-0.
2	1	4.22000E+05	9.00000E+04	2.01250E+08	9.75500E+06	4.46764E+00	-0.
3	3	-0.	-0.	-0.	-0.	3.72303E+00	-0.
4	2	-0.	-0.	-0.	-0.	-0.	1.05880
5	3	-0.	-0.	-0.	-0.	3.72303E+00	-0.
6	1	3.85000E+05	9.20000E+04	2.01250E+08	1.01200E+07	4.46764E+00	-0.
7	3	-0.	-0.	-0.	-0.	3.72303E+00	-0.
8	3	-0.	-0.	-0.	-0.	3.72303E+00	-0.
9	1	3.81000E+05	8.70000E+04	2.01250E+08	1.05000E+07	4.46764E+00	-0.
10	3	-0.	-0.	-0.	-0.	3.72303E+00	-0.
11	2	-0.	-0.	-0.	-0.	-0.	1.05880
12	3	-0.	-0.	-0.	-0.	3.72303E+00	-0.
13	1	4.59000E+05	8.30000E+04	2.01250E+08	1.08700E+07	4.46764E+00	-0.
14	3	-0.	-0.	-0.	-0.	3.72303E+00	-0.
15	3	-0.	-0.	-0.	-0.	3.72303E+00	-0.
16	1	5.55000E+05	8.10000E+04	2.01250E+08	1.11000E+07	4.46764E+00	-0.
17	3	-0.	-0.	-0.	-0.	3.72303E+00	-0.
18	2	-0.	-0.	-0.	-0.	-0.	1.05880
19	3	-0.	-0.	-0.	-0.	3.72303E+00	-0.
20	1	8.04000E+05	7.20000E+04	2.01256E+08	1.15500E+07	4.46764E+00	-0.
21	3	-0.	-0.	-0.	-0.	3.72303E+00	-0.
22	3	-0.	-0.	-0.	-0.	3.72303E+00	-0.
23	1	7.44000E+05	7.50000E+04	2.01250E+08	1.15500E+07	4.46764E+00	-0.
24	3	-0.	-0.	-0.	-0.	3.72303E+00	-0.
25	2	-0.	-0.	-0.	-0.	-0.	1.05880
26	3	-0.	-0.	-0.	-0.	3.72303E+00	-0.
27	1	8.04000E+05	7.20000E+04	2.01250E+08	1.15500E+07	4.46764E+00	-0.
28	3	-0.	-0.	-0.	-0.	3.72303E+00	-0.
29	3	-0.	-0.	-0.	-0.	3.72303E+00	-0.
30	1	8.89000E+05	7.00000E+04	2.01250E+08	1.15500E+07	4.46764E+00	-0.
31	3	-0.	-0.	-0.	-0.	3.72303E+00	-0.
32	2	-0.	-0.	-0.	-0.	-0.	1.05880
33	3	-0.	-0.	-0.	-0.	3.72303E+00	-0.
34	1	8.04000E+05	7.20000E+04	2.01250E+08	1.15500E+07	4.47264E+00	-0.
35	3	-0.	-0.	-0.	-0.	3.72303E+00	-0.
36	3	-0.	-0.	-0.	-0.	3.72303E+00	-0.
37	1	1.03400E+06	6.60000E+04	2.01250E+08	1.15500E+07	4.46764E+00	-0.
38	3	-0.	-0.	-0.	-0.	3.72303E+00	-0.
39	2	-0.	-0.	-0.	-0.	-0.	1.05880
40	3	-0.	-0.	-0.	-0.	3.72303E+00	-0.
41	1	1.13400E+06	6.40000E+04	2.01250E+08	1.15500E+07	4.46764E+00	-0.
42	3	-0.	-0.	-0.	-0.	3.72303E+00	-0.
43	3	-0.	-0.	-0.	-0.	3.72303E+00	-0.
44	1	1.16300E+06	6.30000E+04	2.01250E+08	1.14000E+07	4.46764E+00	-0.
45	3	-0.	-0.	-0.	-0.	3.72303E+00	-0.
46	2	-0.	-0.	-0.	-0.	-0.	1.05880
47	3	-0.	-0.	-0.	-0.	3.72303E+00	-0.
48	1	1.19500E+06	6.20000E+04	2.01250E+08	1.12500E+07	4.46764E+00	-0.
49	3	-0.	-0.	-0.	-0.	3.72303E+00	-0.
50	3	-0.	-0.	-0.	-0.	3.72303E+00	-0.
51	1	1.23600E+06	6.10000E+04	2.01250E+08	1.11500E+07	4.46764E+00	-0.
52	3	-0.	-0.	-0.	-0.	3.72303E+00	-0.
53	2	-0.	-0.	-0.	-0.	-0.	1.05880
54	3	-0.	-0.	-0.	-0.	3.72303E+00	-0.
55	1	1.29500E+06	6.00000E+04	2.01250E+08	1.09500E+07	4.46764E+00	-0.
56	3	-0.	-0.	-0.	-0.	3.72303E+00	-0.
57	3	-0.	-0.	-0.	-0.	3.72303E+00	-0.
58	1	1.32900E+06	6.00000E+04	2.01250E+08	1.08500E+07	4.46764E+00	-0.
59	3	-0.	-0.	-0.	-0.	3.72303E+00	-0.
60	2	-0.	-0.	-0.	-0.	-0.	.50000
61	3	-0.	-0.	-0.	-0.	3.72303E+00	-0.
62	1	1.37900E+06	6.00000E+04	2.01250E+08	1.05700E+07	4.46764E+00	-0.
63	0	-0.	-0.	-0.	-0.	-0.	-0.
64	3	-0.	-0.	-0.	-0.	3.72303E-01	-0.

MANIFOLD $\alpha = 9.2 \times 10^{-5}$; $Z_o = 35.5$ ohms , $V_{mesh\ pt} = 30000$ volts

COUPLING LINE $\alpha = 9.2 \times 10^{-4}$, $Z_o = 50$ ohms

XBL 675-4031

Fig. 16. Table of elements of the full-scale manifold system.

in Hz, and the energy gain in MeV. The seventh column is the length of the manifold section or coupling line in meters, and the last column is the relative power furnished by an amplifier in this location.

The data shown in Fig. 16 are for an ideally tuned manifold system operating at 201.25 MHz except for the numbers in boxes. Here element 30 has a cavity tuned 6 KHz high ($\delta_L Q = 2$), element 34 has a coupling line which is 0.5 cm too long, and element 60 is an amplifier which is furnishing only half of its rated power.

The control cards specify a frequency range in which resonance is expected. The computer starts at an initial frequency and calculates through the 64 matrices summing the power loss and adjusting the amplifiers so that the total power furnished equals the power lost in the loads and in the transmission lines. In order to save computer time, element 63 (with identifying integer 0) is a power balance card which furnishes or absorbs left-over power, and it is equivalent to a load or amplifier in this location. Each end of the manifold is assumed to be short-circuited, so the voltage at the last element should be zero. If it is not zero, the computer steps slightly higher in frequency and calculates through the 64 matrices again, until it detects that the end voltage has passed through zero. At this time a subroutine causes it to home in on the frequency for which the end voltage is nearly zero. It then prints out the frequency and a complete table of values as shown in Figs. 17 and 18. It then resumes the search for another resonance until it has printed a table of values for each resonance in the specified frequency range.

Figure 17 is a table of values for an ideal tuning of the manifold system, and Fig. 18 is a table of values for the set of elements shown in Fig. 16 in which one cavity is detuned, one coupling line is too long, and one amplifier is delivering 50% of normal power. These tables are for a beam current of 50 mA (200 MHz component) at 30 deg phase angle with respect to the voltage across the cavity gap. The converging sequence necessary to satisfy the boundary conditions at the end of the manifold has reduced the voltage at the short circuit to about 20 V out of 30 000 V. Notice that in the column headed MANIFOLD, the mesh-point voltage ranges from 30 000 to 29 936 V, and the phase angle (in units of π radians) has changed by 52 parts in 100 000 along the manifold in Fig. 18. The voltage in the load cavities has not done so well, since the cavities are not so tightly coupled, and the voltage ranges from 29 988 to 29 911 V, with 58 parts in 100 000 phase-angle change. Notice

50 mA

FREQ 2.01250293E+08 HZ

	CAVITY MAGNITUDE	CAVITY ANGLE	MANIFOLD MAGNITUDE	MANIFOLD ANGLE	SWR	POWER	POWER FLOW	VMAX	XMAX
1	0.	0.	3.0000E+04	-1.00000	2.920E+04	0.	4.3418E+02	3.0000E+04	-.7446
2	2.9988E+04	-1.00000	3.0000E+04	-1.00000	1.500E+01	8.4441E+05	8.4484E+05	0.	0.
3	0.	0.	3.0001E+04	.00000	1.493E+01	0.	8.4920E+05	3.0001E+04	-.0004
4	0.	0.	3.0001E+04	.00000	-6.706E+00	-2.7394E+06	-1.8902E+06	0.	0.
5	0.	0.	2.9999E+04	1.00000	-6.721E+00	0.	-1.8858E+06	2.9999E+04	.7442
6	2.9988E+04	-1.00000	2.9999E+04	1.00000	-1.193E+01	8.2316E+05	-1.0626E+06	0.	0.
7	0.	0.	2.9998E+04	-.00000	-1.198E+01	0.	-1.0583E+06	2.9999E+04	-.0010
8	0.	0.	2.9997E+04	1.00000	-1.203E+01	0.	-1.0539E+06	2.9998E+04	.7436
9	2.9986E+04	-1.00000	2.9997E+04	1.00000	-5.804E+01	8.3552E+05	-2.1837E+05	0.	0.
10	0.	0.	2.9997E+04	-.00000	-5.922E+01	0.	-2.1403E+05	2.9998E+04	-.0019
11	0.	0.	2.9997E+04	-.00000	-4.292E+00	-2.7388E+06	-2.9528E+06	0.	0.
12	0.	0.	2.9995E+04	1.00000	-4.298E+00	0.	-2.9483E+06	2.9996E+04	.7426
13	2.9982E+04	-1.00000	2.9995E+04	1.00000	-6.277E+00	9.2937E+05	-2.0189E+06	0.	0.
14	0.	0.	2.9993E+04	-.00001	-6.291E+00	0.	-2.0144E+06	2.9995E+04	-.0029
15	0.	0.	2.9992E+04	.99999	-6.304E+00	0.	-2.0100E+06	2.9994E+04	.7417
16	2.9977E+04	1.00000	2.9992E+04	.99999	-1.300E+01	1.0351E+06	-9.7493E+05	0.	0.
17	0.	0.	2.9991E+04	-.00001	-1.306E+01	0.	-9.7057E+05	2.9994E+04	-.0034
18	0.	0.	2.9991E+04	-.00001	-3.417E+00	-2.7376E+06	-3.7082E+06	0.	0.
19	0.	0.	2.9988E+04	.99999	-3.421E+00	0.	-3.7035E+06	2.9991E+04	.7409
20	2.9972E+04	.99999	2.9988E+04	.99999	-4.933E+00	1.1353E+06	-2.5682E+06	0.	0.
21	0.	0.	2.9986E+04	-.00001	-4.941E+00	0.	-2.5637E+06	2.9990E+04	-.0040
22	0.	0.	2.9984E+04	.99998	-4.949E+00	0.	-2.5592E+06	2.9988E+04	.7406
23	2.9967E+04	.99999	2.9984E+04	.99998	-9.622E+00	1.2428E+06	-1.3164E+06	0.	0.
24	0.	0.	2.9983E+04	-.00002	-9.653E+00	0.	-1.3120E+06	2.9987E+04	-.0042
25	0.	0.	2.9983E+04	-.00002	-3.129E+00	-2.7361E+06	-4.0482E+06	0.	0.
26	0.	0.	2.9979E+04	.99998	-3.132E+00	0.	-4.0434E+06	2.9985E+04	.7400
27	2.9962E+04	.99998	2.9979E+04	.99998	-4.620E+00	1.3023E+06	-2.7411E+06	0.	0.
28	0.	0.	2.9977E+04	-.00002	-4.627E+00	0.	-2.7365E+06	2.9983E+04	-.0047
29	0.	0.	2.9975E+04	.99997	-4.634E+00	0.	-2.7320E+06	2.9980E+04	.7399
30	2.9956E+04	.99997	2.9975E+04	.99997	-9.411E+00	1.3868E+06	-1.3452E+06	0.	0.
31	0.	0.	2.9974E+04	-.00003	-9.441E+00	0.	-1.3408E+06	2.9979E+04	-.0046
32	0.	0.	2.9974E+04	-.00003	-3.106E+00	-2.7345E+06	-4.0753E+06	0.	0.
33	0.	0.	2.9971E+04	.99997	-3.109E+00	0.	-4.0706E+06	2.9977E+04	.7395
34	2.9950E+04	.99997	2.9971E+04	.99997	-4.875E+00	1.4742E+06	-2.5963E+06	0.	0.
35	0.	0.	2.9968E+04	-.00004	-4.882E+00	0.	-2.5918E+06	2.9974E+04	-.0047
36	0.	0.	2.9966E+04	.99996	-4.890E+00	0.	-2.5873E+06	2.9972E+04	.7399
37	2.9945E+04	.99996	2.9966E+04	.99996	-1.197E+01	1.5307E+06	-1.0566E+06	0.	0.
38	0.	0.	2.9965E+04	-.00004	-1.202E+01	0.	-1.0522E+06	2.9971E+04	-.0044
39	0.	0.	2.9965E+04	-.00004	-3.342E+00	-2.7330E+06	-3.7853E+06	0.	0.
40	0.	0.	2.9962E+04	.99996	-3.346E+00	0.	-3.7805E+06	2.9968E+04	.7398
41	2.9940E+04	.99995	2.9962E+04	.99996	-5.881E+00	1.6300E+06	-2.1505E+06	0.	0.
42	0.	0.	2.9961E+04	-.00005	-5.893E+00	0.	-2.1460E+06	2.9965E+04	-.0042
43	0.	0.	2.9959E+04	.99995	-5.905E+00	0.	-2.1416E+06	2.9963E+04	.7405
44	2.9936E+04	.99995	2.9959E+04	.99995	-2.583E+01	1.6521E+06	-4.8947E+05	0.	0.
45	0.	0.	2.9959E+04	-.00005	-2.606E+01	0.	-4.8513E+05	2.9962E+04	-.0037
46	0.	0.	2.9959E+04	-.00005	-3.931E+00	-2.7318E+06	-3.2169E+06	0.	0.
47	0.	0.	2.9956E+04	.99995	-3.936E+00	0.	-3.2123E+06	2.9960E+04	.7407
48	2.9933E+04	.99994	2.9956E+04	.99995	-8.235E+00	1.6772E+06	-1.5351E+06	0.	0.
49	0.	0.	2.9955E+04	-.00005	-8.258E+00	0.	-1.5307E+06	2.9958E+04	-.0033
50	0.	0.	2.9953E+04	.99994	-8.281E+00	0.	-1.5263E+06	2.9956E+04	.7413
51	2.9930E+04	.99994	2.9953E+04	.99994	6.751E+01	1.7135E+06	1.8720E+05	0.	0.
52	0.	0.	2.9954E+04	-.00006	6.599E+01	0.	1.9153E+05	2.9956E+04	-.0027
53	0.	0.	2.9954E+04	-.00006	-4.977E+00	-2.7309E+06	-2.5393E+06	0.	0.
54	0.	0.	2.9952E+04	.99994	-4.985E+00	0.	-2.5348E+06	2.9954E+04	.7418
55	2.9927E+04	.99994	2.9952E+04	.99994	-1.647E+01	1.7674E+06	-7.6739E+05	0.	0.
56	0.	0.	2.9951E+04	-.00006	-1.656E+01	0.	-7.6305E+05	2.9952E+04	-.0020
57	0.	0.	2.9950E+04	.99994	-1.665E+01	0.	-7.5870E+05	2.9951E+04	.7426
58	2.9926E+04	.99993	2.9950E+04	.99994	1.222E+01	1.7929E+06	1.0342E+06	0.	0.
59	0.	0.	2.9951E+04	-.00006	1.217E+01	0.	1.0385E+06	2.9952E+04	-.0012
60	0.	0.	2.9951E+04	-.00006	-7.468E+00	-2.7304E+06	-1.6919E+06	0.	0.
61	0.	0.	2.9950E+04	.99994	-7.487E+00	0.	-1.6875E+06	2.9950E+04	.7434
62	2.9925E+04	.99993	2.9950E+04	.99994	8.830E+01	1.8306E+06	1.4308E+05	0.	0.
63	0.	0.	2.9950E+04	.99994	2.573E+14	-1.4308E+05	4.0296E-08	0.	0.
64	0.	0.	1.7937E+01	.99994	2.573E+14	0.	4.0296E-08	2.9950E+04	-.3724

XBL 675-4032

Fig. 17. Table of values for the ideal full-scale manifold system.

FREQ 2.0125C614E+C8 HZ

	CAVITY MAGNITUDE	CAVITY ANGLE	MANIFOLD MAGNITUDE	MANIFOLD ANGLE	SWR	POWER	POWER FLOW	VMAX	XMIX
1	C.	0.	3.0000E+04	-1.00000	2.920E+04	0.	4.3418E+02	3.0000E+04	-.7446
2	2.9988E+04	.99997	3.0000E+04	-1.00000	1.501E+01	8.4441E+05	8.4484E+05	0.	0.
3	C.	0.	3.0001E+04	.00000	1.493E+01	0.	8.4920E+05	3.0005E+04	.0041
4	C.	0.	3.0001E+04	.00000	-6.183E+00	-2.8999E+06	-2.0507E+06	0.	0.
5	C.	0.	2.9999E+04	-1.00000	-6.156E+00	0.	-2.0463E+06	3.0004E+04	-.7404
6	2.9988E+04	.99997	2.9999E+04	-1.00000	-1.038E+01	8.2316E+05	-1.2231E+06	0.	0.
7	C.	0.	2.9998E+04	.00001	-1.041E+01	0.	-1.2187E+06	3.0015E+04	.0081
8	C.	0.	2.9997E+04	-.99999	-1.045E+01	0.	-1.2143E+06	3.0014E+04	-.7365
9	2.9986E+04	.99998	2.9997E+04	-.99999	-3.353E+01	8.3550E+05	-3.7884E+05	0.	0.
10	C.	0.	2.9997E+04	.00001	-3.352E+01	0.	-3.7448E+05	3.0032E+04	.0115
11	C.	0.	2.9997E+04	.00001	-3.881E+00	-2.8991E+06	-3.2736E+06	0.	0.
12	C.	0.	2.9994E+04	-.99999	-3.886E+00	0.	-3.2690E+06	3.0031E+04	-.7323
13	2.9981E+04	.99999	2.9994E+04	-.99999	-5.439E+00	9.2931E+05	-2.3397E+06	0.	0.
14	C.	0.	2.9992E+04	.00002	-5.449E+00	0.	-2.3352E+06	3.0056E+04	.0157
15	C.	0.	2.9990E+04	-.99998	-5.458E+00	0.	-2.3307E+06	3.0054E+04	-.7289
16	2.9976E+04	.99999	2.9990E+04	-.99998	-9.844E+00	1.0350E+06	-1.2957E+06	0.	0.
17	C.	0.	2.9985E+04	.00003	-9.817E+00	0.	-1.2913E+06	3.0092E+04	.0198
18	C.	0.	2.9989E+04	.00003	-3.047E+00	-2.8976E+06	-4.1889E+06	0.	0.
19	C.	0.	2.9985E+04	-.99996	-3.050E+00	0.	-4.1841E+06	3.0100E+04	-.7227
20	2.9967E+04	-.99919	2.9985E+04	-.99996	-4.917E+00	1.3029E+06	-2.8813E+06	0.	0.
21	C.	0.	2.9983E+04	-.00000	-4.925E+00	0.	-2.8762E+06	3.1713E+04	-.0804
22	C.	0.	2.9981E+04	.99996	-4.933E+00	0.	-2.8712E+06	3.1711E+04	.6642
23	2.9964E+04	.99992	2.9981E+04	.99996	-8.554E+00	1.2426E+06	-1.6286E+06	0.	0.
24	C.	0.	2.9980E+04	-.00006	-8.579E+00	0.	-1.6238E+06	3.1449E+04	-.0732,
25	C.	0.	2.9980E+04	-.00008	-3.114E+00	-2.8960E+06	-4.5198E+06	0.	0.
26	C.	0.	2.9977E+04	.99989	-3.117E+00	0.	-4.5144E+06	3.1606E+04	.6637
27	2.9959E+04	.99984	2.9977E+04	.99989	-4.297E+00	1.3021E+06	-3.2123E+06	0.	0.
28	C.	0.	2.9975E+04	-.00015	-4.303E+00	0.	-3.2073E+06	3.1304E+04	-.0713
29	C.	0.	2.9972E+04	.99982	-4.309E+00	0.	-3.2023E+06	3.1301E+04	.6733
30	2.9953E+04	.99977	2.9972E+04	.99982	-7.419E+00	1.3866E+06	-1.8158E+06	0.	0.
31	C.	0.	2.9971E+04	-.00021	-7.458E+00	0.	-1.8110E+06	3.1049E+04	-.0632
32	C.	0.	2.9971E+04	-.00021	-2.91CE+00	-2.8942E+06	-4.7053E+06	0.	0.
33	C.	0.	2.9968E+04	.99975	-2.913E+00	0.	-4.7000E+06	3.1177E+04	.6739
34	2.9976E+04	.99874	2.9968E+04	.99975	-3.937E+00	1.3013E+06	-3.3964E+06	0.	0.
35	C.	0.	2.9965E+04	-.00027	-3.942E+00	0.	-3.3915E+06	3.0811E+04	-.0576
36	C.	0.	2.9963E+04	.99970	-3.947E+00	0.	-3.3866E+06	3.0808E+04	.6870
37	2.9942E+04	.99965	2.9963E+04	.99970	-7.104E+00	1.5303E+06	-1.8563E+06	0.	0.
38	C.	0.	2.9961E+04	-.00033	-7.121E+00	0.	-1.8517E+06	3.0597E+04	-.0489
39	C.	0.	2.9961E+04	-.00033	-2.795E+00	-2.8923E+06	-4.7440E+06	0.	0.
40	C.	0.	2.9958E+04	.99965	-2.797E+00	0.	-4.7389E+06	3.0676E+04	.6895
41	2.9935E+04	.99959	2.9958E+04	.99965	-4.201E+00	1.6295E+06	-3.1094E+06	0.	0.
42	C.	0.	2.9955E+04	-.00038	-4.207E+00	0.	-3.1047E+06	3.0452E+04	-.0442
43	C.	0.	2.9953E+04	.99960	-4.213E+00	0.	-3.0999E+06	3.0450E+04	.7005
44	2.9930E+04	.99955	2.9953E+04	.99960	-8.922E+00	1.6515E+06	-1.4485E+06	0.	0.
45	C.	0.	2.9952E+04	-.00042	-8.949E+00	0.	-1.4440E+06	3.0290E+04	-.0357
46	C.	0.	2.9952E+04	-.00042	-2.989E+00	-2.8905E+06	-4.3345E+06	0.	0.
47	C.	0.	2.9949E+04	.99957	-2.992E+00	0.	-4.3296E+06	3.0325E+04	.7049
48	2.9926E+04	.99951	2.9949E+04	.99957	-4.835E+00	1.6764E+06	-2.6532E+06	0.	0.
49	C.	0.	2.9947E+04	-.00045	-4.843E+00	0.	-2.6486E+06	3.0177E+04	-.0300
50	C.	0.	2.9945E+04	.99953	-4.850E+00	0.	-2.6440E+06	3.0175E+04	.7146
51	2.9921E+04	.99948	2.9945E+04	.99953	-1.368E+01	1.7125E+06	-9.3154E+05	0.	0.
52	C.	0.	2.9944E+04	-.00048	-1.374E+01	0.	-9.2715E+05	3.0074E+04	-.0221
53	C.	0.	2.9944E+04	-.00048	-3.341E+00	-2.8850E+06	-3.8161E+06	0.	0.
54	C.	0.	2.9941E+04	.99951	-3.344E+00	0.	-3.8114E+06	3.0083E+04	.7204
55	2.9917E+04	.99945	2.9941E+04	.99951	-6.199E+00	1.7662E+06	-2.0452E+06	0.	0.
56	C.	0.	2.9939E+04	-.00050	-6.212E+00	0.	-2.0407E+06	3.0001E+04	-.0154
57	C.	0.	2.9938E+04	.99949	-6.225E+00	0.	-2.0363E+06	3.0000E+04	.7292
58	2.9913E+04	.99943	2.9938E+04	.99949	-5.160E+01	1.7914E+06	-2.4490E+05	0.	0.
59	C.	0.	2.9938E+04	-.00051	-5.253E+01	0.	-2.4057E+05	2.9954E+04	-.0078
60	C.	0.	2.9938E+04	-.00051	-7.817E+00	-1.3637E+06	-1.6043E+06	0.	0.
61	C.	0.	2.9936E+04	.99948	-7.858E+00	0.	-1.5999E+06	2.9953E+04	.7367
62	2.9911E+04	.99942	2.9936E+04	.99948	5.511E+01	1.8289E+06	2.2906E+05	0.	0.
63	C.	0.	2.9936E+04	.99948	2.572E+14	-2.2906E+05	2.6864E-08	0.	0.
64	C.	0.	2.0068E+01	.99948	5.143E+14	0.	1.3432E-08	2.9936E+04	-.3725

XBL 675-4033

Fig. 18. Table of values for the perturbed full-scale manifold system.

also that from Fig. 17 to Fig. 18 the perturbations in the system have pulled the resonant frequency by approximately 300 Hz. The resonant frequency differs from 2.0125000×10^8 because the beam loading is at a 30-deg phase angle. The voltage maximum is 31 713 V in the manifold adjacent to the detuned cavity, and the position of the voltage maximum has moved about 8 cm from the mesh point. The standing-wave ratio varies between about 3 and 30 along the manifold, depending on the power flowing in a given section. The power delivered to the cavities ranges from about 0.84 MW to 1.8 MW, which is about 0.4 MW per cavity more than the copper losses.

There is a small error in these tables because the converging procedure doesn't reduce the voltage at the short circuit completely to zero. However, one can compare the relative values of the ideally tuned case with the case of a particular combination of perturbations to find the deviation from perfect voltage lock that might result in a full-scale system. The deviations in amplitude and voltage lock are in good agreement with the theory given in the first sections of this paper.

REFERENCES

1. H. G. Hereward and P. Lapostolle,, Energy Flow and Transients in the Alvarez Structure, in Proceedings of the V International Conference on High Energy Accelerators, Frascati, 1965, p. 742.
2. T. Nishikawa, A Study of Field Distribution and Beam Loading in Proton Linacs at High Energies, IEEE Trans. Nucl. Sci. NS-12, 630 (1965).
3. A. Carne, G. Dome, N. Fewell, and W. Jüngst, Development of the Cross-Bar Structure for a Proton Linear Accelerator, in Proceedings of the V International Conference on High Energy Accelerators, Frascati, 1965, p. 624.
4. E. A. Knapp, P. W. Allison, C. R. Emigh, L. N. Engel, J. M. Potta, and W. J. Shlaer, Accelerating Structure Research at Los Alamos, in Proceedings of the 1966 Linear Accelerator Conference, Los Alamos Report LA-3609, 1966, p. 83.
5. S. Giordano and J. P. Hannwacker, Measurement on a Multistem Drift Tube Structure, in Proceedings of the 1966 Linear Accelerator Conference, Los Alamos Report LA-3609, 1966, p. 88.
6. G. Schaffer, High Power UHF Components for Desy, Paper presented at Particle Accelerator Conference, in Washington, March 10-12, 1965.
7. Reference Data for Radio Engineers, Fourth Edition (International Telephone and Telegraph Co., Ch. 5 Sect. 19.)
8. E. Ginzton, Microwave Measurements (McGraw-Hill Book Co., New York, 1957), Sec. 7.2.